

## MULTIPLE FALL OF PŘÍBRAM METEORITES PHOTOGRAPHED

### 1. Double-Station Photographs of the Fireball and Their Relations to the Found Meteorites

Zd. Ceplecha, Astronomical Institute of the Czechoslovak Academy of Sciences, Ondřejov

Received August 6, 1960

The double-station photographs with rotating-shutter cameras of the multiple meteoritic fall at Příbram (Czechoslovakia) on 7th April, 1959, are the basis of this paper. The vertical projection in geographical coordinates and heights of the main trajectory, of 16 other fragment trajectories, into which the meteorite was splitting, and of all significant points of these trajectories are given in this paper. The velocities of the main body and of one fragment are determined. The light curve was derived. The original velocity and radiant yield the orbit. The actions in connection with the search for meteorites are described. Four meteorites of total mass of 5.80 kg were found. The "Hojšín" meteorite was found only 12 m apart from the trace, which was computed and staked out in the territory previously. The places of meteorite falls are given in geographical coordinates. The correspondences between photographed fragment-trajectories and meteorites are determined on the base of the "dark-flight" distance from the end of light trajectory to the position of the corresponding meteorite. The dark-flight distances were calculated for different  $s_E/m_E$  and  $h_E$  using step-by-step integration of motion equations and considering the relatively strong variable wind at different heights. The drag coefficients  $\Gamma$  for  $M \geq 6$  were found in the range 0.5 to 1. The masses of the not found meteorites were computed by different ways and with different results. The preliminary results of paper [7], based on the correspondences of vertical projections of trajectories to the meteorite places only, are not confirmed by this paper. The total mass of all the meteorites and especially the mass of the main body which reached the ground are very uncertain.

*Метеоритный дождь Пржебрам снято фотографиями. 1. Базисные фотографии болида и их связь с метеоритами.* В работе приведены результаты обработки базисных фотографий падения метеоритного дождя вблизи г. Пржибрам (Чехословакия) 7 апреля 1959 г. Приведена отвесная проекция траектории основного тела, траекторий 16 осколков, и значимых точек на этих траекториях на поверхность Земли в географических координатах. Приведены также высоты точек траекторий над уровнем моря. Вычислена скорость одного осколка и основного тела по измерениям перерывов полученных обтюратором. Определена кривая света. Первоначальная скорость и радиант были использованы для вычисления орбиты. Все операции связанные с отысканием метеоритов описаны в главе 2 настоящей работы. Четыре найденных метеорита имели общую массу весом в 5,80 кг. Метеорит „Гойшин“ был найден на расстоянии примерно 12 м от отвесной проекции его траектории, которая была раньше вычислена и зарисована в области падения. Места падений метеоритов приведены в географических координатах. На основании „длины добега“ метеоритов (от точки погасания болида до места падения метеорита) была определена связь между траекториями отдельных сфотографированных осколков и между местами нахождения метеоритов. Длина добега вычислена для различных значений  $s_E/m_E$  и  $h_E$  при помощи численного решения дифференциальных уравнений движения. Влияние сильного ветра на различных высотах до 20 км было тоже учтено. Коэффициент сопротивления для метеоритов при  $M \geq 6$  находится в пределах 0,5–1. Было установлено, что теоретически определенные массы не найденных метеоритов были различны для разных методов их определения. Результаты работы [7], основанной только на отвесных проекциях траекторий и их связи с метеоритами, не были подтверждены. Определение общей массы всех метеоритов а в частности массы основного не найденного тела не надежны.

#### Introduction

On 7th April, 1959 at 19<sup>h</sup>30<sup>m</sup>20<sup>s</sup> to 27<sup>s</sup> UT a bright fireball of —19th absolute magnitude illuminated the Czech territory. A multiple meteoritic fall near Příbram followed this fireball [8]. The meteor cameras used for systematical meteor photography were in action on this night at the Ondřejov Observatory and at the second station, Prčice, and the trajectories of falling meteorites were photographed at both the stations. This result is more valuable, since the Ondřejov cameras are provided with rotating shutters, and the velocity of the falling meteorite and its changes could be determined. The progressive separation of the body into the 17 pieces of the multiple meteoritic fall was also photographed.

Our attention during the reduction of "meteoritic" plates was directed to the region of the meteorite fall, which was well defined one week after the fall on the basis of photographic results. Four stony meteorites of total mass 5.80 kg were found by volunteers from local inhabitants as the result of our work in the territory.

For the first time the accurate photographic results can be completed by the measurements made directly with the cosmical body.

#### 1. Photographs of the meteorites fall

##### 1.1 Cameras and plates

Double-station meteor photography at the Ondřejov Observatory has been carried out from the year 1951 quite systematically with 5 cameras and since the year 1955 with 10 cameras at each station. These ten cameras cover about 1/2 of the visible sky hemisphere. From the beginning of this programme till the night of meteorite photographs about 2500 hours of exposure were made by the whole equipment. If this time is transferred in the period 1951 to 1955 to the function of 10 cameras, we establish that about 1700 hours of exposure of 1/2 of the visible hemisphere were necessary to photograph the meteorite fall.

Ten unguided cameras at the Ondřejov Observatory have objectives Tessar 1 : 4.5, f = 18 cm. Agfa ISS plates 21/10 Din of 9 × 12 cm dimensions are used. The cameras are situated below two rotating shutters each with two arms. Since the beginning of the year 1959 the number of rotations has been controlled by means of a printing chronograph, which is driven by a crystal clock. The accuracy of relative time determinations is thus greater than the accuracy of measurement of the breaks.

The velocity is then determined absolutely without any additional error from the time determinations. The meteorite fall was photographed by 3 different cameras at Ondřejov.

Twelve additional guided cameras are used at the Ondřejov Observatory for the determination of the passage time of meteors. Cameras are guided automatically. The time of the passage is thus measured to a precision of 1 sec. The meteorite fall was photographed by two of these guided cameras. One guided camera, which was directed near the horizon at the time of the meteorite fall, photographed a part of the observatory building illuminated by the meteorite's light.

The second station Prčice 40·388 km from Ondřejov is equipped with 10 unguided cameras without rotating shutters. These cameras together with the Ondřejov unguided cameras determine the total geometry of the trajectory, and the velocity. The meteorite, passing almost through the zenith of Prčice, was photographed by 5 cameras at this station.

All the cameras are equipped with special shutters, which are used for the precise beginning and end of the exposure. An accuracy of  $\pm 0.2$  sec is sufficient and fully satisfies the lower limit of position accuracy of the plates ( $\pm 3''$ ).

A more detailed description of our meteor stations was published in papers [1] and [2]. In contrast to the data in paper [1] the number of rotations of rotating shutters was changed to about 1400 rotations per minute at the time of the meteorite fall.

A list of all plates with trails of the meteorite fall is given in Table 1. The height intervals over which the trajectory was photographed, the number of breaks, the number of individual trajectories, and the time of beginning of the exposure to which all data during the computations were related, are given for each plate.

Table 1  
The list of "meteorite" plates, 1959, April 7

Plate No.	Station	camera	rotating shutter	height interval [km] from to	number of breaks	number of trails	beginning of the exposure UT**) h m s
1924	On	u	+	97·8–68	92	1	19 13 57·9
1926	On	u	+	84 –39	149	1	19 13 27·9
1928	On	u	+	41 –31	0*) (10)	2	19 13 27·9
P 1924	P	u	—	97·8–71	—	1.	19 09 37·6
P 1926	P	u	—	80 –40	—	1	19 10 05·1
P 1922	P	u	—	37 –30	—	9	19 09 37·6
P 1928	P	u	—	34 –27	—	8	19 10
P 1927	P	u	—	32 –22	—	12	19 10 05·1
G 886	On	g	—	97·8–65	—	1	19 14
G 888	On	g	—	74 –38	—	1	19 14
G 891	On	g	building illuminated by the meteorite light				

u ... unguided camera  
g ... guided camera

+ with rotating shutter  
— without rotating shutter

\*) the breaks are only on the fragment trail.

\*\*) All the computations were made for the beginning of the exposure of plate 1926. Right ascension on other plates were corrected for this time. On the other hand all the data in tables of this paper are referred to the time of "meteorite passage" 19<sup>h</sup>30<sup>m</sup>21<sup>s</sup>3.

## 1.2 Photographic processing

All plates were developed by rapid metol (4 gr) — hydrochinon (7 gr) developer as used for normal meteor plates from other nights. The time of development was 12 min. at 20°C.

The density of the sky on the plates was very high in the neighbourhood of the meteorite trajectory because of the great illumination of the very sensitive plates at focal ratio 1 : 4·5. The plates were almost completely opaque, and thus not suitable for direct measurements. The negative plates could be used only for the measurement of the beginning of the trail on plates 1924, P 1924, and G 886. The other negative plates were subjected to further photographic processing. Contact glassy copies were made using the same Agfa ISS 21/10 Din plates. The illumination of a 100 W bulb at the distance of about 30 cm was used with an exposure time of a few seconds. The positive image on the plate was then used for the measurement. The precision of the measurements on positive plates was practically the same as on normal negative plates ( $\pm 10''$  to  $\pm 3''$ ).

## 1.3 Measurement and reduction of the plates

The measurement of the plates was performed using a Zeiss "Koordinatenmessgerät" which allows complete exploitation of the plate accuracy. The measurement of each point was repeated four times, two measurements in one position of the plate and two measurements with the plate optically turned through 180° (without changing the coordinate system). The measurement of straight-line formations was performed in a series of points and the straight-line was put through them by the method of least squares.

A relative lack of stars on the plates was caused by the overexposure. When it was possible, the method of 3 stars was used for the reduction of plates [3], [4], [5]. The detailed method of plate reduction is given in paper [1]. The plates 1924, P 1924, 1928, P 1922, P 1927, and G 886 were reduced by this method of 3 stars.

Plate P 1928 was not used at all, because the defect of the shutter made an accurate determination of the beginning of the exposure impossible. The part of the meteorite trajectory exposed on this plate is also exposed on plates P 1922 and P 1927. Thus this height interval is not missing.

Plates 1926 and P 1926 were not suitable for the 3 stars to be found. The method of 2 stars was used for these plates. The optical centre in coordinates RA and Dec was taken over from the calculations of three-star method made for another plate previously exposed in the same camera. This exposure before 7th April, 1959, was chosen as near to this night as was possible. In this section this plate is called the reference plate.

The reduction method is then modified from the method of paper [1] as follows:

- The right ascension and declination  $\alpha_0, \delta_0$  of the optical centre is taken from the reference plate.
- The equations of paper [4] are used for the computation of  $\cos \varepsilon_i$  ( $i = 1, 2$ ). ( $\varepsilon_i$  is the angular distance of the reference star  $i$  from the plate centre.)

c) The focal distance is computed by means of  $\cos \varepsilon_i$ . A good check of the computation is the agreement with the focal distance computed previously for the reference plate.

d) The optical centre in the rectangular coordinate system  $x_0, y_0$  is then computed from equations of paper [3].

The remainder of the computation is as in the method of three stars [1].

The practical computation for plates 1926 and P 1926 showed that the precision using the two-star method is the same as for the three-star method. The condition must be fulfilled that the unguided cameras do not change their directions or focal lengths between the exposures of the reference and measured plates.

The reduction of plates provides in this case accurate determinations of geographical coordinates of individual points of the meteorite trajectory. This method of reduction will be given in detail in Sections 1.8, 1.9, 1.10.

#### 1.4 Geographical positions of stations

The geographical coordinates of the local geodetical system must be used for all calculations, if the results are to be staked out on the ground. Such coordinates were introduced in the past in Czechoslovakia by Křovák [6] using the Bessel ellipsoid with

$$a' = 6377.397 \text{ km}, \quad e'^2 = 0.0066744$$

This is the reason for using the starting coordinates of both the stations throughout the following calculations in the system related to the Bessel ellipsoid. Thus the precise distances and directions were measured relatively to the earth surface, and also relatively to the positions of our cameras. Differences between these directions and those measured relatively to the stars could exist. The old geodetical net of Křovák for Czechoslovakia on Bessel ellipsoid was transformed by shifting and turning to the corrected system of local geodetical coordinates, which we use in our computations. The transformation to this corrected system was performed on the basis of astronomical measurements at some tens of trigonometric points of the first order. The directions in this corrected system of geographical coordinates are consistent with the star system, therefore the differences are less than it is possible to measure with the accuracy of our cameras. We calculate all geographical coordinates with the precision corresponding to an error in relative distances of less than 1 metre.

The corrected geographical coordinates related to the Bessel ellipsoid are exclusively given in this paper. Its relative accuracy is greater than 1 metre, the precision which we wish to keep when measuring the relative position of cameras at Ondřejov and Prčice and when staking out the points of meteorite trajectory on the ground. The absolute precision according to the whole ellipsoid is of course less.

All geodetical measurements made in the territory were facilitated by the fact that a very dense net of trigonometrical points of lower orders is present in Czechoslovakia. It was possible to find a suitable trigonometrical point in all cases not farther than 2 km from the measured point or trajectory. Geodetical measurements were taken with a Wild theodolite.

Geographical coordinates of the stations are as follows:

Ondřejov	$\varphi_{On} = 49^{\circ}54'36''\cdot07$
	$\lambda_{On} = 14^{\circ}46'57''\cdot16$ E. Gr.
	$h_{On} = 0.530 \text{ km}$
	$R_{On} = 6365.493 \text{ km}$

Prčice	$\varphi_P = 49^{\circ}34'49''\cdot85$
	$\lambda_P = 14^{\circ}32'49''\cdot20$
	$h_P = 0.423 \text{ km}$
	$R_P = 6365.507 \text{ km}$

Relative position

$$\begin{aligned} d_{On,P} &= 40.388 \text{ km} \\ t_s &= 31^{\circ}26'13'' \\ \delta_s &= -36^{\circ}02'25'' \end{aligned}$$

The following geocentric rectangular coordinates were used for the calculation in Section 1.8

$$\begin{aligned} x_P &= -3285.2377 \\ y_P &= +2524.6519 \\ z_P &= +4832.4974 \end{aligned}$$

These coordinates hold for local sidereal time

$$\vartheta_P = 142^{\circ}27'29''\cdot90$$

The values  $x_P, y_P, z_P, \alpha$  and  $\vartheta$  were used during the calculations for the time of the beginning of the corresponding exposure. The values given in this paper are all transformed to the time of meteorite passage ( $19^{\text{h}}30^{\text{m}}21^{\text{s}}$ ) and in this form they are given in the tables and text of all sections.

#### 1.5 Apparent trajectories, radiants, and time of passage

Individual parts of trajectories were derived by the method given above from plates of both stations. The parts of the trajectory were chosen so that it was possible to use the linear relation in one part for the calculation of the apparent mean trajectory. Thus the apparent trajectory is in each part represented by a great circle on the sky. Each part of the trajectory is denoted by the end number of the plate and by the index of series numbers of the part on that plate.

The great circle on the sphere can be written in RA, Dec system of coordinates\*)

$$(1) \quad \sin(\varrho - \alpha) = \cot \psi \tan \delta$$

The values  $\varrho$  and  $\cot \psi$  determined from the plates are given in Table 2 for the main trajectory, for its different parts with different mean height. The value  $\varrho$  is given for the time of meteorite passage, though it was used for the time of exposure beginning during all calculations.

Table 3 contains the apparent trajectories of fragment No. 15 which is the only one for which double-station records are available. Table 4 contains apparent trajectories (great circles) of all other fragments which were photographed at Prčice only.

It is possible to state clearly how the meteorite was photographed at different heights, using the survey of apparent trajectories in this section and Table 1.

\*) A list of mathematical symbols used throughout the paper (also in tables) is at the end of the paper.

Table 2  
Apparent great circles and radiants of the main trajectory No. 1

$*h$ [km]	$\alpha_r$	Ondřejov		Prčice		Radiant		Part No.
		$\varrho$	$\cot \psi$	$\varrho$	$\cot \psi$	$\alpha_R$	$\delta_R$	
82.9	176.4	107 20 38	-2.6280	25 26 05	-0.72485	189 34 28	20 39 29	4
74.5	174.3	107 20 24	-2.6277	25 25 30	-0.72420	189 34 39	20 39 38	$6_1$
58.2	167.0	107 25 15	-2.6240	25 21 54	-0.72322	189 31 19	20 40 52	$6_2$
44.3	152.8	107 29 10	-2.6184	25 19 46	-0.72280	189 27 59	20 42 55	$6_3$
36.8	137.0	107 26 12	-2.6292	25 12 14	-0.72334	189 23 46	20 38 11	8
	104.8			25 17 21	-0.72496			$7_1$
	90.7			25 31 09	-0.72401			$7_2$
	82.7			25 39 44	-0.72291			$7_3$

\*) Mathematical symbols used in tables are at the end of the paper.

Table 3  
Apparent great circles and radiant of double-station fragment No. 15

$h$ [km]	$\alpha_r$	Ondřejov		Prčice		Radiant		$\delta_R$
		$\varrho$	$\cot \psi$	$\varrho$	$\cot \psi$	$\alpha_R$	$\delta_R$	
36.1	135.1	108 16 08	-2.5170	26 05 44	-0.72911	189 27 41	21 26 08	

Table 4  
Apparent great circles of the fragments, which were exposed at Prčice only

Trail No.	$\alpha_r$	$\varrho$	$\cot \psi$	Trail No.	$\alpha_r$	$\varrho$	$\cot \psi$
2	98.3	24 53 05	-0.72542	8	89.1	25 38 53	-0.72510
	95.2	25 00 13	-0.72492	9	87.7	25 59 26	-0.71947
	90.4	25 08 07	-0.72425	10	121.7	24 00 05	-0.71791
	86.0	25 26 22	-0.72221		118.6	24 28 57	-0.71853
	83.5	25 23 41	-0.72252		115.7	23 43 18	-0.71804
	81.5	25 23 53	-0.72249		111.2	23 29 08	-0.71900
3	104.7	25 51 26	-0.72505	11	118.6	24 27 40	-0.72024
	90.1	25 56 52	-0.72416		109.9	24 34 50	-0.72145
	86.1	25 50 12	-0.72484	12	130.2	24 56 26	-0.72058
	84.4	25 49 22	-0.72494		124.2	25 19 16	-0.72149
	82.4	25 51 03	-0.72471		110.0	25 03 10	-0.72222
4	116.7	25 45 17	-0.72520	13	126.4	23 52 32	-0.71490
	105.8	25 41 39	-0.72636	14	132.0	24 17 15	-0.71518
5	90.1	25 12 17	-0.72500	16	130.8	26 10 50	-0.73103
6	85.7	26 28 52	-0.71836	17	118.5	28 26 06	-0.72782
7	81.9	28 16 46	-0.70175				
	80.3	29 05 24	-0.69409				

The main trajectory: was photographed from the beginning at a height of 97.8 km to 31 km at both the stations. The breaks are measurable down to 40 km height. Photographs from Prčice only are available from a height of 31 km to 22 km. The end of the main trajectory is off the plates.

Fragment No.15: double station photograph with measurable breaks in the height range 37 to 35 km.

All other fragments: one-station photographs from Prčice only. The end of trajectories Nos. 2, 3, 4, 7 are off the plates, the remaining 12 fragment trajectories have the ends of their trajectories on the plates.

The fragments No. 10, 12, 13, 14, 15, and 16 ought to be visible on the Ondřejov plate 1928. These fragments are well separated and visible on Prčice plates. Only fragment No.15 is seen on the Ondřejov plate. The cause of this is that the corresponding part of the main trajectory of the bolide is almost twice as near to Prčice as to Ondřejov. The bolide passed close to the zenith of Prčice. The trails of the fragments are thus merging on the Ondřejov plate 1928 with the trail of the main body.

It is possible to see that for these fragments the differences of their heights from that of the main trajectory must be very small. Greater differences in height would appear in the "side view" from Ondřejov as a separation of the fragment trails from the main one.

The radiants are directly determined by the apparent trajectories. The apparent positions of the radiants of individual parts of the main trajectory are given in Table 2. The radiant for fragment No. 15 is in Table 3. The change of direction of the trajectory during the meteorite flight is clearly shown in Table 2. This change is used in Section 1.15 in the calculation of the original radiant.

The time of the fireball appearance was determined by the method given in paper [2]. The time interval from the beginning of exposure of plate 1924 to the time of the fireball passage was derived by comparison of apparent trajectories from plates 1924 and G 886, that is from unguided and guided plate. The resulting time of the fireball passage

$$t = 19^{\text{h}} 30^{\text{m}} 21^{\text{s}} \text{ UT}$$

is determined with a precision of about  $\pm 1^{\text{s}}$  according to the inaccuracy of guiding the camera [2]. This time holds for the mean point on plate 1924, or about  $1^{\text{s}}$  after the beginning of the fireball. The time interval of the fireball assuming its duration (Section 1.7) is from  $19^{\text{h}} 30^{\text{m}} 20^{\text{s}}$  to  $27^{\text{s}}$  UT.

### 1.6 The basic points on the main trajectory, and on fragment No.15

A basic point was chosen in each part of the main trajectory where a calculation of the velocity was possible. The velocity can be computed very simply using this basic point. The distance of the basic point from the camera and the position of the image of this point on the plate determine the real distances measured along the trajectory from the basic point. The Millman relation is used for the calculation of these real distances [4]

$$(2) \quad l = k \frac{l'}{l' + n}$$

The real distances together with the time of individual breaks then determine the velocity. The distances of the

basic points from Ondřejov and Prčice, their heights above sea-level, and their right ascensions and declinations as obtained directly from the double-station plates are given in Table 5. The distances and coordinates of the basic points were calculated according to [4] and the heights were determined using the rectangular geocentric coordinates.

A good measured break near to the mean point of each part of the trajectory was chosen as the basic point.

### 1.7 The velocities

Equation (2) was used for the determination of the real distances of individual breaks from the corresponding basic point directly from the distances measured on the

Table 5  
The distances of basic points for the double-station trajectories

Part. No.	Trajectory No.	$\alpha_{on}$	$\delta_{on}$	$\alpha_p$	$\delta_p$	$r_{on}$ [km]	$r_p$ [km]	$h$ [km]
4	1	162 03 30	17 15 20	178 14 18	32 13 58	112.950	107.371	92.042
6 <sub>1</sub>	1	154 49 42	15 40 13	174 16 40	35 32 06	90.779	83.073	74.536
6 <sub>2</sub>	1	144 22 43	12 54 19	166 59 13	40 38 39	72.023	61.177	58.174
6 <sub>3</sub>	1	131 02 31	8 40 40	152 50 22	47 39 37	59.048	44.201	44.286
8	15	120 48 08	4 55 40	135 07 59	52 21 25	53.603	35.825	36.092

Table 6  
Measured breaks of the main trail No. 1

Plate 1924

Break No.	$l$ [km]	$\Delta l$ [km]	Break No.	$l$ [km]	$\Delta l$ [km]	Break No.	$l$ [km]	$\Delta l$ [km]
2	-6.1641		33	7.4237	0.4369	64	20.9607	0.4382
3	-5.6939		34	7.8545	0.4355	65	21.4093	0.4372
4	-5.2356		35	8.2959	0.4375	66	21.8454	0.4340
5	-4.8075		36	8.7473	0.4366	67	22.2793	0.4357
6	-4.3779		37	9.1754	0.4374	68	22.7140	0.4389
7	-3.9537	0.4399	38	9.6127	0.4367	69	23.1619	0.4372
8	-3.5150	0.4380	39	10.0389	0.4373	70	23.5944	0.4359
9	-3.0645	0.4348	40	10.4845	0.4373	71	23.9951	0.4339
10	-2.6148	0.4360	41	10.9203	0.4355	72	24.4532	0.4364
11	-2.1983	0.4378	42	11.3511	0.4382	73	24.9010	0.4378
12	-1.7650	0.4388	43	11.7906	0.4353	74	25.3331	0.4348
13	-1.3139	0.4380	44	12.2276	0.4379	75	25.7685	0.4353
14	-0.8873	0.4376	45	12.6690	0.4367	76	26.1840	0.4381
15	-0.4471	0.4350	46	13.1025	0.4368	77	26.6431	0.4371
16	0.0000	0.4370	47	13.5572	0.4381	78	27.0918	0.4391
17	0.4339	0.4384	48	13.9653	0.4369	79	27.5100	0.4367
18	0.8655	0.4354	49	14.4182	0.4370	80	27.9473	0.4350
19	1.3120	0.4384	50	14.8512	0.4375	81	28.3759	0.4389
20	1.7354	0.4388	51	15.2886	0.4369	82	28.8244	0.4367
21	2.1719	0.4360	52	15.7319	0.4356	83	29.2923	0.4364
22	2.6195	0.4365	53	16.1596	0.4368	84	29.7001	0.4374
23	3.0398	0.4378	54	16.5974	0.4362	85	30.1189	0.4370
24	3.4962	0.4372	55	17.0438	0.4371	86	30.5727	0.4378
25	3.9408	0.4374	56	17.4718	0.4367	87	31.0099	0.4350
26	4.3602	0.4382	57	17.9130	0.4364	88	31.4553	0.4355
27	4.7988	0.4358	58	18.3335	0.4353	89	31.8841	
28	5.2440	0.4384	59	18.7803	0.4363	90	32.3170	
29	5.6842	0.4358	60	19.2222	0.4366	91	32.7541	
30	6.1091	0.4355	61	19.6553	0.4374	92	33.1747	
31	6.5542	0.4387	62	20.0962	0.4366	93	33.6470	
32	6.9773	0.4377	63	20.5122	0.4380			

Table 6 (continued)

Plate 1926

Part 6<sub>1</sub>

Break No.	$l$ [km]	$\Delta l$ [km]	Break No.	$l$ [km]	$\Delta l$ [km]	Break No.	$l$ [km]	$\Delta l$ [km]
2	-13.5159		19	-6.0985	0.4350	36	1.3046	0.4352
3	-13.0845		20	-5.6583	0.4354	37	1.7318	0.4357
4	-12.6379		21	-5.2220	0.4349	38	2.1768	0.4357
5	-12.1951		22	-4.7861	0.4370	39	2.6127	0.4330
6	-11.7471		23	-4.3528	0.4345	40	3.0260	0.4348
7	-11.3156	0.4381	24	-3.9212	0.4350	41	3.4773	0.4337
8	-10.8899	0.4372	25	-3.4856	0.4353	42	3.9187	0.4342
9	-10.4566	0.4366	26	-3.0517	0.4347	43	4.3572	0.4355
10	-10.0157	0.4356	27	-2.5954	0.4348	44	4.7692	0.4342
11	-9.5803	0.4346	28	-2.1800	0.4353	45	5.2199	0.4336
12	-9.1351	0.4350	29	-1.7487	0.4360	46	5.6412	0.4363
13	-8.7121	0.4365	30	-1.3055	0.4358	47	6.0735	0.4337
14	-8.2717	0.4358	31	-0.8747	0.4356	48	6.5318	
15	-7.8392	0.4357	32	-0.4381	0.4327	49	6.9547	
16	-7.4007	0.4358	33	0.0000	0.4357	50	7.3623	
17	-6.9652	0.4349	34	0.4391	0.4361	51	7.8406	
18	-6.5252	0.4359	35	0.8720	0.4332	52	8.2558	

Table 6 (continued)

Part 6<sub>2</sub>

Break No.	$l$ [km]	$\Delta l$ [km]	Break No.	$l$ [km]	$\Delta l$ [km]	Break No.	$l$ [km]	$\Delta l$ [km]
43	-19.5461		71	-7.3686	0.4329	99	4.7915	0.4349
44	-19.1335		72	-6.9588	0.4365	100	5.2216	0.4356
45	-18.6821		73	-6.5244	0.4321	101	5.6473	0.4337
46	-18.2603		74	-6.0611	0.4368	102	6.0992	0.4356
47	-17.8274		75	-5.6385	0.4334	103	6.5012	0.4335
48	-17.3684	0.4339	76	-5.1977	0.4342	104	6.9644	0.4341
49	-16.9448	0.4378	77	-4.7595	0.4364	105	7.3914	0.4327
50	-16.5366	0.4363	78	-4.3327	0.4375	106	7.8257	0.4331
51	-16.0577	0.4381	79	-3.9021	0.4347	107	8.2762	0.4306
52	-15.6419	0.4350	80	-3.4694	0.4354	108	8.6849	0.4356
53	-15.2074	0.4358	81	-3.0265	0.4319	109	9.1328	0.4318
54	-14.7556	0.4351	82	-2.5946	0.4342	110	9.5487	0.4322
55	-14.3193	0.4373	83	-2.1494	0.4333	111	9.9787	0.4339
56	-13.8796	0.4310	84	-1.7144	0.4351	112	10.4053	0.4314
57	-13.4777	0.4348	85	-1.2840	0.4345	113	10.8576	0.4316
58	-13.0102	0.4361	86	-0.8786	0.4333	114	11.2827	0.4327
59	-12.5934	0.4337	87	-0.4170	0.4350	115	11.7131	0.4341
60	-12.1634	0.4350	88	0.0000	0.4358	116	12.1648	0.4325
61	-11.7478	0.4353	89	0.4488	0.4330	117	12.5907	0.4329
62	-11.2934	0.4353	90	0.8754	0.4319	118	13.0010	0.4321
63	-10.8464	0.4356	91	1.3065	0.4368	119	13.4601	0.4320
64	-10.4187	0.4324	92	1.7559	0.4338	120	13.8900	0.4330
65	-9.9689	0.4360	93	2.2081	0.4350	121	14.3038	
66	-9.5269	0.4379	94	2.6158	0.4343	122	14.7341	
67	-9.1246	0.4335	95	3.0349	0.4346	123	15.1786	
68	-8.6539	0.4322	96	3.4889	0.4341	124	15.6028	
69	-8.2698	0.4358	97	3.9207	0.4343	125	16.0435	
70	-7.8036	0.4330	98	4.3498	0.4293			

plate  $l'$ . These distances  $l$  are given in Table 6 for different plates and different parts of the main trajectory. The measurement of breaks was not as accurate as usual, because of extreme overexposure. This inaccuracy was reduced by the great number of measurable breaks. Therefore the differences of distances were computed between ten breaks, and the result was used for the mean break of these ten. Such computation will yield the "smooth" differences  $\Delta l$  for all measured breaks excepting the first

and last five. The differences of distances  $\Delta l$  are given in Table 6, each difference is in the row of the mean break of the ten from which it was computed.

The mean velocities were derived from the mean  $\Delta l$  as the corresponding time interval  $\Delta t$  can be considered constant. A straight line was drawn through the values of  $\Delta l$ , the slope of which determines the deceleration independent of the velocity, and the mean value of  $\Delta l$  which determines the velocity. Thus the mean errors are de-

Table 6 (continued)

Part 6<sub>3</sub>

Break No.	$l$ [km]	$\Delta l$ [km]	Break No.	$l$ [km]	$\Delta l$ [km]	Break No.	$l$ [km]	$\Delta l$ [km]
116	-8.1467		128	-2.9539	0.4295	140	2.1496	0.4258
117	-7.7204		129	-2.5472	0.4294	141	2.5534	0.4248
118	-7.3099		130	-2.1249	0.4265	142	2.9980	0.4250
119	-6.8504		131	-1.6947	0.4254	143	3.3884	0.4261
120	-6.4202		132	-1.2714	0.4274	144	3.8607	0.4158
121	-6.0062	0.4329	133	-0.8358	0.4221	145	4.2578	0.4180
122	-5.5756	0.4304	134	-0.4127	0.4275	146	4.6846	
123	-5.1308	0.4346	135	0.0000	0.4274	147	5.1066	
124	-4.7063	0.4303	136	0.4363	0.4248	148	5.5177	
125	-4.2654	0.4295	137	0.8569	0.4269	149	5.8855	
126	-3.8177	0.4312	138	1.2570	0.4224	150	6.3300	
127	-3.4168	0.4304	139	1.7282	0.4273			

Relation between the numbers of breaks on plate 1924 and on plate 1926: Break No. 68.40 of plate 1924 = break No. 27.00 of plate 1926

Corresponding breaks of plates 1924 and 1926 at other points can be derived by means of the rotating-shutters speed from Table 7.

Table 7  
Mean velocities and decelerations

Plate No.	Mean break No.	$t$ [sec]	$h$ [km]	Least square solution		Number of breaks	$f$ [br/sec]	$\Delta t$ [sec]	$\frac{dv}{dt}$ eq. (17) [km/sec <sup>2</sup> ]
				$v$ [km/sec]	$dv/dt$ [km/sec <sup>2</sup> ]				
1924	27.5	0.00000	88.594	20.887 $\pm 0.009$	-0.031 $\pm 0.035$	42	47.782 $\pm 0.005$	0.020928 $\pm 0.000002$	-0.001 $-0.002$
	68.5	0.85806	76.289	20.864 $\pm 0.010$	0.000 $\pm 0.039$				
1926	27.0	0.85602	76.318	20.860 $\pm 0.007$	-0.113 $\pm 0.030$	41	47.930 $\pm 0.005$	0.020864 $\pm 0.000002$	-0.002 $-0.006$
	69.0	1.73230	63.837	20.838 $\pm 0.013$	-0.100 $\pm 0.049$				
	105.5	2.49383	52.970	20.773 $\pm 0.013$	-0.207 $\pm 0.071$	30			-0.014 $-0.018$
	115.0	2.69203	50.164	20.717 $\pm 0.013$	-0.370 $\pm 0.068$				
	133.0	3.06758	44.858	20.459 $\pm 0.024$	-1.08 $\pm 0.16$	25			

terminated for velocities and also decelerations. The results of the least square solution are given in Table 7, together with the number of breaks per second. This number of breaks per second was derived from direct measurements of duration of 448 rotations of the rotating shutter by means of a printing chronograph. The two values in Table 7 correspond to the two different rotating shutter used.

The velocity at a height of 76 km was computed from two different cameras with two different rotating shutters. The very good agreement of these two velocities shows the great accuracy of the mean velocities of Table 7.

On the other hand the decelerations measured at a height of 76 km in the two determinations differ by more than the limits of mean errors. The mean errors in the case of decelerations are of the same order as the decelerations. It is possible to explain the difference between the above mentioned values by small real decelerations for such a large body. The method of computation of the deceleration after smoothing the data over 10 breaks is not suitable for the direct determination of the deceleration.

Thus the mean errors must be taken much greater than the computed values given in Table 7. Only one value of deceleration has any real meaning from this point of view, it is for the height of 45 km, where the deceleration of -1.08 was measured independently of the velocity.

The deceleration may also be deduced from the velocities of Table 7, and the method will be given in Section 1.15. In this case the velocity must be given as a known function of height. The deceleration computed using relation (17) of Section 1.15 is given in Table 7 for comparison. These decelerations determined from the velocities of Table 7 are very small and can hardly be determined directly from the break measurements. The directly determined decelerations of Table 7 (least square method) are only fictitious values, which are given systematical deviations due to the smoothing over 10 breaks.

The measurement of the breaks on the trajectory of fragment No. 15 is given in Table 8. The mean values for this double-station fragment are given at the end of this table.

The observed velocity was extrapolated to lower

heights on some theoretical assumptions with the aim to determine the duration of the fireball. The duration

6·8 sec

results by numerical integration, if  $v_E$  is supposed 7 km/sec and the height  $h_E = 13\cdot3$  km used.

Table 8  
Measured breaks, mean velocities and decelerations  
of fragment No. 15  
Plate 1928

Break No.	$l$ [km]	$\Delta l$ [km]	Break No.	$l$ [km]	$\Delta l$ [km]
2	-2.0133	0.3323	7	-0.3164	0.3164
3	-1.6810	0.3567	8	0.0000	0.3320
4	-1.3243	0.3502	9	0.3320	0.3312
5	-0.9741	0.3321	10	0.6632	0.2919
6	-0.6420	0.3256	11	0.9551	
Mean break No.	$h$ [km]	$v$ [km/sec]	$\frac{dv}{dt}$ [km/sec <sup>2</sup> ]	number of breaks	$f$ [br/sec]
6.5	36.435	15.76 $\pm 0.22$	-11 $\pm 4$	9	47.782 $\pm 0.005$

### 1.8 The reference trajectory

A straight line trajectory was chosen in the very close vicinity of the real meteorite trajectory. This straight trajectory is called the reference trajectory. It is then possible to express the position of individual points of the main trajectory and of the trajectories of fragments by means of deviations from the reference trajectory. This is very suitable because the apparent trajectory goes almost through the zenith of the Prčice station. The trajectories of all the fragments are then easily determined from the one-station record of the Prčice station, using the method of deviations from the reference trajectory.

Part two of the main trajectory from plates 1926 and P 1926 ( $6_2$ ) was chosen as the reference trajectory. In this calculation Prčice is taken as the basic station, because many fragments are visible on the Prčice plates and these are the subject of computation in later sections.

The great circle of the apparent reference trajectory is given by:

$$(3) \quad \varrho_r = 25^\circ 21' 54'' \quad \cot \psi_r = -0.72322$$

We choose  $\alpha_r$ . Then from the equation of the apparent trajectory (1) we obtain the declination of the chosen point on the reference trajectory  $\delta_r$ , using the values (3). The numerical choice of  $\alpha_r$  is evident from Table 9, and was calculated at short intervals, which are necessary if we wish to use the table for interpolation. The values  $\alpha_r$  were chosen in the original computation as the whole numbers in degrees, but they are given in Table 9 transformed to the time of meteorite passage.

Table 9  
The reference trajectory

$\alpha_r$	$\delta_r$	$r_r$ [km]	$\lambda_r$	$\varphi_r$	$h_r$ [km]
° / ' / "	° / ' / "	° / ' / "	° / ' / "	° / ' / "	
180 14 03	30 25 19	127.832	15 27 41.31	49 21 52.26	106.593
178 14 03	32 14 00	107.447	15 16 08.00	49 24 45.72	92.109
176 14 03	33 56 41	93.303	15 07 58.60	49 26 47.27	81.964
174 14 03	35 33 32	82.940	15 01 53.85	49 28 17.38	74.444
172 14 03	37 04 44	75.036	14 57 10.85	49 29 27.02	68.633
170 14 03	38 30 29	68.827	14 53 24.47	49 30 22.53	64.000
168 14 03	39 51 00	63.827	14 50 18.81	49 31 07.95	60.210
163 14 03	42 50 51	54.788	14 44 32.16	49 32 32.48	53.158
156 14 03	46 16 38	46.897	14 39 10.55	49 33 50.56	46.642
152 14 03	47 53 09	43.789	14 36 55.70	49 34 23.20	43.919
149 14 03	48 56 36	41.888	14 35 29.74	49 34 43.98	42.184
144 14 03	50 26 53	39.313	14 33 27.59	49 35 13.48	39.724
137 14 03	52 04 14	36.584	14 31 07.81	49 35 47.17	36.913
128 14 03	53 25 47	34.045	14 28 42.25	49 36 22.19	33.991
119 14 03	54 03 45	32.198	14 26 39.77	49 36 51.61	31.536
109 14 03	53 58 06	30.683	14 24 38.68	49 37 20.65	29.113
99 14 03	53 01 31	29.578	14 22 44.55	49 37 47.98	26.832
89 14 03	51 08 47	28.821	14 20 50.11	49 38 15.34	24.549
84 14 03	49 48 20	28.576	14 19 50.52	49 38 29.57	23.361
80 14 03	48 30 48	28.452	14 19 00.77	49 38 41.45	22.370
76 14 03	47 00 19	28.401	14 18 08.51	49 38 53.91	21.330
72 14 03	45 15 33	28.438	14 17 12.97	49 39 07.15	20.225
68 14 03	43 14 58	28.580	14 16 13.25	49 39 21.37	19.038
65 14 03	41 33 09	28.772	14 15 25.04	49 39 32.85	18.080
62 14 03	39 40 45	29.053	14 14 33.22	49 39 45.18	17.052
59 14 03	37 37 01	29.442	14 13 37.07	49 39 58.53	15.938
56 14 03	35 21 11	29.965	14 12 35.66	49 40 13.11	14.721
47 14 03	27 15 01	32.713	14 08 46.49	49 41 07.44	10.186
44 14 03	24 05 35	34.221	14 07 08.34	49 41 30.66	8.248
38 14 03	17 07 01	38.746	14 02 58.35	49 42 29.68	3.322
36 14 03	14 36 48	40.899	14 01 12.45	49 42 54.62	1.240

The distance from the station to the point on the reference trajectory  $r_r$  is then determined by the equations

$$(4) \quad r_r = \frac{r_0}{\sin \omega_{rR}}$$

$$(5) \quad \cos \omega_{rR} = \sin \delta_r \sin \delta_R + \cos \delta_r \cos \delta_R \cos (\alpha_r - \alpha_R)$$

The constant  $r_0$  in relation (4) is the nearest distance of the reference trajectory to the Prčice station, and it is possible to determine it from the distance of an arbitrary point on the reference trajectory. Such distance is the double-station distance determined from Table 5 for the trajectory  $6_2$ , which was chosen as the reference one. Using the coordinates  $\alpha_P, \delta_P$  from Table 5 and relations (4) and (5), we obtain

$$r_0 = 28.4008 \text{ km}$$

This value of  $r_0$  and the relation (4) were used for the computation of the distances  $r_r$  from the Prčice station as they are given in Table 9.

The geocentric coordinates  $R_r, \varphi'_r, \vartheta_r$  of individual points of the reference trajectory can be obtained from the relations

$$(6) \quad \begin{aligned} R_r \cos \varphi'_r \cos \vartheta_r &= x_P + r_r \cos \alpha_r \cos \delta_r \\ R_r \cos \varphi'_r \sin \vartheta_r &= y_P + r_r \sin \alpha_r \cos \delta_r \\ R_r \sin \varphi'_r &= z_P + r_r \sin \delta_r, \end{aligned}$$

where the adopted numerical values of  $x_P, y_P, z_P$  are given in Section 1.4. The following relation holds for eastern longitudes

$$(7) \quad \vartheta_r - \vartheta_P = \lambda_r - \lambda_P$$

Thus the difference of computed  $\vartheta_r$  from  $\vartheta_P$  gives directly the difference in longitudes from the Prčice station, that is the longitude of the chosen point on the reference trajectory contained in Table 9.

The geocentric latitude  $\varphi'$  was transferred to the geographical latitude using the Bessel ellipsoid (the same one used for the calculation of  $x_P, y_P, z_P$ ). These geographic latitudes are given in Table 9, but they do not correspond with the vertical projection of the point on the reference trajectory onto the surface. The correction of the latitude to the vertical projection will be given in the next chapter.

The height  $h_r$  of the chosen point on the reference trajectory is given by the radius vector  $R_r$ . The height is given in Table 9 in kilometres as the height above sea-level.

### 1.9 The real trajectory of the main part

A smooth change in the parameters of the apparent trajectory is necessary for the determination of the deviations of the real trajectory from the reference one. The directly determined values  $\varrho$  and  $\cot \psi$  from Table 2 were used. The independent variable chosen was  $\alpha_r$ . The result of the smooth dependences together with direct measured values is in Fig. 1. The values used for the calculation of the deviations from the reference trajectory are given in Table 10 for the values of  $\alpha_r$  used in Table 9.

The advantage of this method of calculation is evident

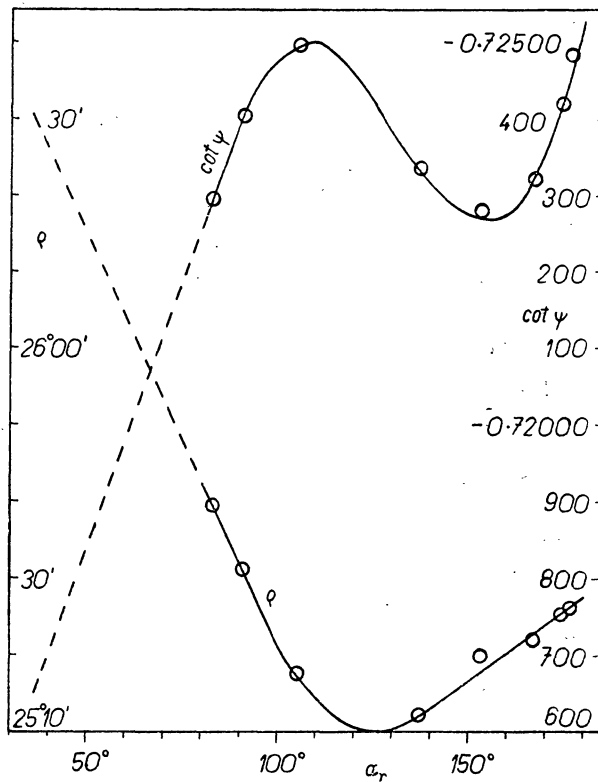


Fig. 1. Great circle parameters  $\varrho$ ,  $\cot \psi$  of the apparent main trajectory as the function of the reference apparent right ascension from Prčice.

Table 10  
The main trajectory No. 1

$\varrho$	$\cot \psi$	$D_\alpha$	$D_\delta$	$D_\varphi$	$D_\theta$	$D_{\varphi'}$	$\lambda$	$\varphi$	$h$ [km]
25 27 21	-0.72532	24	21	0.54	0.31	-11.44	15 27 41.62	49 21 41.36	106.479
25 26 39	-0.72491	19	17	0.37	0.20	-9.88	15 16 08.20	49 24 36.21	92.022
25 25 57	-0.72453	17	15	0.28	0.15	-8.79	15 07 58.75	49 26 38.76	81.896
25 25 15	-0.72418	17	16	0.25	0.13	-7.98	15 01 53.98	49 28 09.65	74.389
25 24 33	-0.72387	17	16	0.23	0.12	-7.36	14 57 10.97	49 29 19.89	68.590
25 23 51	-0.72359	18	18	0.23	0.12	-6.85	14 53 24.59	49 30 15.90	63.965
25 23 09	-0.72334	19	20	0.24	0.12	-6.46	14 50 18.93	49 31 01.73	60.182
25 21 21	-0.72292	14	17	0.16	0.08	-5.70	14 44 32.24	49 32 26.94	53.143
25 18 57	-0.72266	2	3	0.02	0.01	-5.00	14 39 10.56	49 33 45.58	46.640
25 17 33	-0.72269	-8	-19	-0.13	-0.03	-4.71	14 36 55.67	49 34 18.36	43.921
25 16 33	-0.72277	-9	-40	-0.26	-0.02	-4.52	14 35 29.72	49 34 39.20	42.190
25 14 45	-0.72296	3 03	-2 09	-0.78	1.13	-4.26	14 33 28.72	49 35 08.44	39.734
25 12 21	-0.72332	-2 04	-1 41	-0.54	-0.73	-3.96	14 33 07.08	49 35 42.67	36.929
25 10 09	-0.72393	-1 33	-2 44	-0.80	-0.70	-3.64	14 28 41.55	49 36 17.75	34.011
25 10 57	-0.72454	-0 51	-3 18	-0.90	-0.70	-3.38	14 26 39.07	49 36 47.33	31.562
25 14 45	-0.72498	0 06	-3 36	-0.94	-0.68	-3.12	14 24 38.00	49 37 16.59	29.143
25 22 03	-0.72472	0 57	-3 18	-0.85	-0.59	-2.88	14 22 43.96	49 37 44.25	26.867
25 32 45	-0.72381	1 52	-3 31	-0.92	-0.62	-2.63	14 20 49.49	49 38 11.79	24.588
25 38 03	-0.72311	2 27	-3 50	-1.02	-0.68	-2.50	14 19 49.84	49 38 26.05	23.402
25 42 27	-0.72256	3 15	-4 30	-1.23	-0.81	-2.40	14 18 59.96	49 38 37.82	22.413
25 46 45	-0.72200	4 23	-5 27	-1.53	-1.00	-2.29	14 18 07.51	49 38 50.09	21.375
25 51 03	-0.72145	5 55	-6 44	-1.95	-1.26	-2.17	14 17 11.71	49 39 03.03	20.272
25 55 21	-0.72090	7 53	-8 20	-2.51	-1.61	-2.04	14 16 11.64	49 39 16.82	19.087
25 58 39	-0.72048	9 41	-9 44	-3.03	-1.93	-1.94	14 15 23.11	49 39 27.88	18.131
26 01 57	-0.72006	11 45	-11 18	-3.66	-2.32	-1.83	14 14 30.90	49 39 39.69	17.106
26 05 09	-0.71964	14 03	-12 59	-4.38	-2.76	-1.71	14 13 34.31	49 39 52.44	15.994
26 08 27	-0.71923	16 40	-14 51	-5.25	-3.29	-1.58	14 12 32.37	49 40 06.28	14.779
26 18 15	-0.71798	25 47	-21 10	-8.92	-5.49	-1.09	14 08 41.00	49 40 57.43	
26 21 33	-0.71756	29 13	-23 30	-10.65	-6.51	-0.88	14 07 01.83	49 41 19.13	
26 27 57	-0.71673	36 19	-28 21	-15.23	-9.19	-0.36	14 02 49.16	49 42 14.09	
26 30 09	-0.71646	38 47	-30 03	-17.27	-10.36	-0.13	14 01 02.09	49 42 37.22	

These data are listed in the same sequence and for the same points  $\alpha_r$  as in Table 9.

from the fact that at the end of the photographed trajectory the one-station plates P 1922 and P 1927 dominantly control the results. It is necessary to point out that the meteorite trajectory was not photographed up to the very end of the main trajectory, and thus the values for  $\alpha_r < 80^\circ$  in Table 10 are only extrapolated.

The deviation of the real trajectory from the reference one is expressed relatively simply, because the apparent trajectory passes almost exactly through the zenith of the Prčice station. If we wish to obtain the deviation always perpendicularly to the reference trajectory, it is possible in this particular case to write quite simply

$$(8a) \quad r_r = \text{const.}$$

which is the condition holding exactly in the case of the precise passage of the reference trail through the zenith. The difference from the zenith is so small that only the point for  $\alpha_r = 144^\circ$  (near to the zenith) is influenced significantly by the chosen method. The relation (8a) together with the passage through zenith will yield another important relation for the perpendicular deviation

$$(8b) \quad h_r = \text{const.}$$

Thus the conditions of calculation of the perpendicular deviations from the reference trajectory are much simplified. If we denote the small deviations

$$(9) \quad \begin{aligned} D_\alpha &= \alpha - \alpha_r \\ D_\delta &= \delta - \delta_r \\ D_\varphi &= \varphi - \varphi_r \\ D_\theta &= D_\lambda = \vartheta - \vartheta_r \end{aligned}$$

then by differentiating relations (6) with (8a) and (8b):

$$(10a) \quad R_r = R + h_r$$

$$(10) \quad \frac{D_\varphi}{D_\delta} = \frac{r_r \cos \delta_r}{R_r \cos \varphi'_r}$$

$$(11) \quad \frac{D_\lambda}{D_\delta} = \frac{D_\varphi}{D_\delta} = \frac{r_r [\sin \delta_r - \cos \delta_r \tan \varphi'_r \cos (\vartheta_r - \alpha_r)]}{R_r \cos \varphi'_r \sin (\vartheta_r - \alpha_r)}$$

$$(12) \quad \frac{D_\alpha}{D_\delta} = \frac{\tan \delta_r \cos (\vartheta_r - \alpha_r) - \tan \varphi'_r}{\sin (\vartheta_r - \alpha_r)}$$

$$(13) \quad \begin{aligned} D_\delta &= \\ &= \frac{\sin (\varrho - \alpha_r) - \tan \delta_r \cot \psi}{\frac{D_\alpha}{D_\delta} \cos (\varrho - \alpha_r) + \sin (\varrho - \alpha_r) \tan \delta_r + \cot \psi} \end{aligned}$$

In these relations  $\varrho$  and  $\cot \psi$  hold for the real observed not smooth trajectory.

All these four corrections are given in Table 10. If we use only  $D_\varphi$  for the correction of  $\varphi_r$ , we do not obtain the vertical projection onto the ground. The correction for the vertical projection  $D'_\varphi$  is easy to determine, using the relation

$$(14) \quad D'_\varphi = \frac{h_r}{R_r} (\varphi'_r - \varphi_r),$$

which gives the deviation of the vertical line from the radius vector at the height  $h_r$ . The geographical latitude of the vertical projection of the real trajectory is then given by

$$(15) \quad \varphi = \varphi_r + D_\varphi + D'_\varphi$$

and is listed in Table 10. The longitude of the vertical projection of the point on the real trajectory is computed from the corresponding reference longitude using relation (9), and is listed in Table 10.

The deviations of the reference and real trajectory in height must be determined after finishing all the above mentioned computations, because the perpendicular deviation of  $D_\varphi$ ,  $D_\theta$  to the reference trajectory requires the condition (8b) of constant height to be fulfilled. In addition it is necessary to correct the reference height  $h_r$  and to compute the real height  $h$  from the relation

$$(16) \quad D_h = h - h_r.$$

The real heights from Table 5 and the reference heights determine  $D_h$ , which is given in Fig. 2 as a function of  $\lambda_r$ .

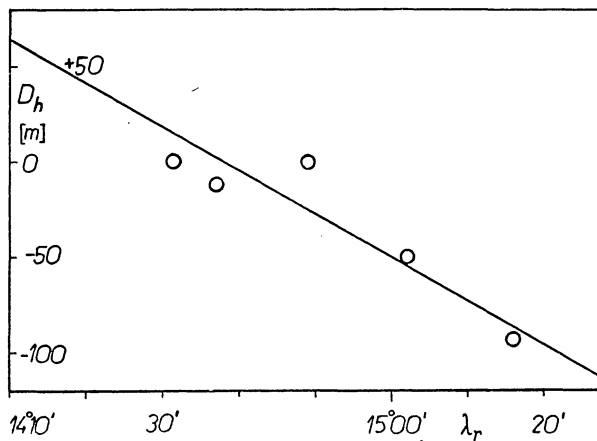


Fig. 2. Residuals  $D_h$  of height in metres as the function of the reference geographical longitude  $\lambda_r$ . The mean straight line was used for the correction of "reference heights" to actual heights.

Through the scattered direct observed points it is necessary to draw a smooth curve. A linear relation was used in this particular case. The heights of the real trajectory were determined using the smooth  $D_h$  from Fig. 2 and are given in Table 10.

The residuals in height  $h$  (smooth values) are given in Table 11 as a function of the observed heights (Tab. 5). The residuals are very small, and it is evident that the accuracy of the chosen method of reduction is sufficient. Analogical residua for  $\varphi$  and  $\lambda$  are practically near to zero, because the smooth dependence of  $\varrho$  and  $\cot \psi$  on  $\alpha_r$

Table 11  
Residua  $\Delta h$  for the main trajectory

$h_{obs}$ [km]	$h_{sm}$ [km]	$\Delta h$ [km]
92.042	92.047	-0.005
74.536	74.530	+0.006
58.174	58.149	+0.025
44.286	44.301	-0.015
36.814	36.828	-0.014

$h_{obs}$  height directly from the double-station plates  
 $h_{sm}$  height derived by means of reference trajectory and smooth values of  $\varrho$

passes almost exactly all observed points. Thus the directly determined  $\varphi$  and  $\lambda$  from the double-station plates for the mean point of each trajectory part are the same as the smooth values obtained by the method of the reference trajectory. The importance of the method of reference trajectory lies in the possibility of using the one-station trajectories for the computation.

### 1.10 The real trajectories of fragments

The continuous separation of individual fragments from the main (or parent fragment) trajectory is visible and measurable on plates P 1922, P 1928, P 1927, and 1928, beginning with the height of 44 km. All trajectories of individual fragments, excepting No. 15, which has the double-station trajectory, were photographed only

from one station — Prčice. The heights of these one-station fragments cannot differ too much from the heights of corresponding points of the main trajectory, as the trails must then be separated on the Ondřejov plate, too. This was mentioned in Section 1.5. It is possible to take advantage of the fact that the trajectory passes almost through the zenith of Prčice, and the sight from beneath determines directly the vertical projection of fragments trajectories. The condition of small difference in heights between the main trajectory and those of individual fragments can be substituted by the condition of constant height (8b). The condition (8a) holds and the method of deviations from the reference trajectory can also be used for the determination of the fragments trajectories. Thus the one station plates of all fragments can be used as double-station ones.

As the starting value the parameters of the apparent

Table 12  
Deviations  $D$  of the fragments trajectories from the reference trajectory (metres)

$\lambda_r$	$h$ [km]	Trajectory No.								
		1	10	11	12	13	14	15	16	17
14 37	44.01	-138							-139	
14 36	42.80	-138							-149	
14 35	41.59	-138							-159	
14 34	40.39	-138							-170	
14 33	39.18	-138							-180	
14 32	37.98	-137							-191	
14 31	36.77	-136							-202	
14 30	35.57	-135							-212	
14 29	34.37	-134							-223	
14 28	33.17	-132	-55							
14 27	31.97	-130	-27							
14 26	30.77	-127	-6	-49						
14 25	29.57	-123	+23	-28						
14 24	28.37	-118	+66	-6						
14 18	21.21	[-120]	[+328]			[+332]				
14 17	20.02	[-131]	[+372]			[+332]				[m]

$\lambda_r$	$h$ [km]	Trajectory No.								
		1	2	3	4	5	6	7	8	9
14 27	31.97	-130		-131	-132					
14 26	30.77	-127		-136	-141					
14 25	29.57	-123		-141	-150					
14 24	28.37	-118		-145	-159					
14 23	27.18	-113	-100	-150	-168	-110				
14 22	25.98	-112	-80	-155	-176	-101				
14 21	24.78	-108	-70	-160	-183	-92				
14 20-5	24.19	-107	-70	-162	-186					
14 20	23.59	-107	-71	-164	-188					
14 19-5	22.99	-109	-74	-166	-190					
14 19	22.40	-111	-78	-168	-191					
14 18	21.21	[-120]	[-95]	[-172]	[-193]					
14 17	20.02	[-131]	[-119]	[-177]	[-195]					
14 16	18.82	[-146]	[-150]	[-182]	[-198]					
14 15	17.64	[-165]	[-186]	[-186]	[-200]					
14 14	16.45	[-187]	[-226]							
14 13	15.26	[-210]	[-270]							
14 12	14.07	[-238]	[-319]							
14 11	12.89	[-266]	[-374]							
14 07		[-383]								
14 01		[-582]								

sign + deviation to the right (north) of the reference trajectory } in metres  
 sign - deviation to the left (south) of the reference trajectory } in metres  
 [ ] extrapolated values.

Table 13  
Direct measurements of curved trail No. 2 on plate  
P 1927

$x$ [mm]	$y$ [mm]	$x$ [mm]	$y$ [mm]
57	5.7320 ± 0.0013	30	5.9262 ± 0.0033
55	5.7585 ± 0.0015	28	5.9285 ± 0.0021
52	5.7744 ± 0.0027	26	5.9300 ± 0.0023
50	5.8013 ± 0.0025	24	5.9354 ± 0.0014
48	5.8148 ± 0.0024	22	5.9338 ± 0.0023
46	5.8296 ± 0.0026	20	5.9295 ± 0.0023
44	5.8348 ± 0.0015	18	5.9383 ± 0.0015
42	5.8596 ± 0.0013	16	5.9542 ± 0.0023
40	5.8714 ± 0.0006	14	5.9528 ± 0.0017
38	5.8814 ± 0.0019	12	5.9515 ± 0.0016
36	5.8872 ± 0.0027	10	5.9474 ± 0.0004
34	5.8928 ± 0.0014	8.9	5.9437 ± 0.0018
32	5.9063 ± 0.0022		

$x, y$  are the rectangular coordinates obtained directly by the "Koordinatenmessgerät"

trajectories  $\varrho$  and  $\cot \psi$  determined directly from the plates were used. (Tab. 4.) Only one pair  $\varrho$  and  $\cot \psi$

(corresponding to one apparent great circle) was used for most of the weak fragments. The brighter trails of fragments were in some cases distinctly curved. In such cases the trajectory was separated into several parts and straight lines were put through the measured points in these parts. (Tab. 4) The same procedure of smoothing the observed dependence of  $\varrho$  and  $\cot \psi$  on  $\alpha_r$  was used as for the main trajectory. The change of parameters  $\varrho$  and  $\cot \psi$  well define the course of the trajectory with  $\alpha_r$ , and it is possible to use this change for extrapolation to the invisible dark part of the trajectory.

The relations (9) to (13) were used and the correction for the vertical projection were computed from (14). The results are given in Table 12, where are contained the perpendicular deviations  $D$  from the reference trajectory expressed in metres. These data represent for each fragment the position of the vertical projection of its trajectory to the ground. The perpendicular deviations of the main trajectory No. 1 from the reference trajectory are given for the sake of completeness, too. The deviations have a positive sign when they are to the right side (north), and a negative sign when they are to the left side (south) of the reference trajectory. The longitudes  $\lambda_r$  in Table 12

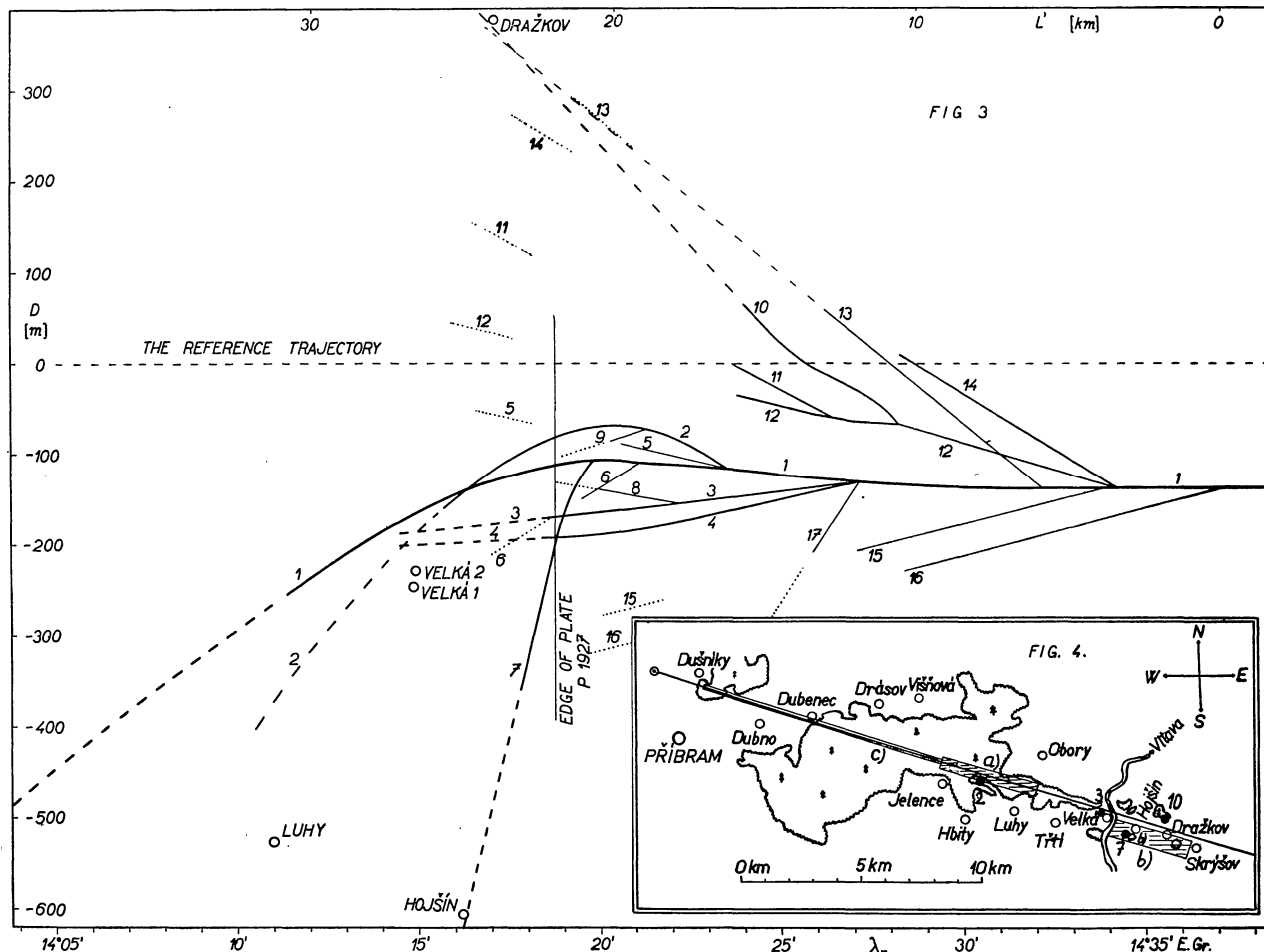


Fig. 3. Vertical ground projection of individual meteorite trajectories. The dimensions on the  $y$ -axis are very much enlarged against the  $x$ -axis. Thus the curvatures and inclinations of individual trajectories are much greater than in reality. — the luminous trajectory, - - - the extrapolated dark-flight trajectory, ○ place of meteorite finds, .... probable places of the not found meteorites. The reference trajectory is represented by the line  $D = 0$ .

Fig. 4. Schematic map of the "meteorite region" contains the villages, forests, the river Vitava, places 2, 3, 7, 10 of the found meteorites, and the trajectory of the main body. In the left upper corner there is the intersection of the reference trajectory with the ground. The regions a), b), c) are explained in the paper.

were taken sufficiently close to permit an accurate representation of the trajectories of all fragments. The corresponding geographical latitudes  $\varphi_r$  of the reference trajectory, which are necessary when one wishes to express the geographical latitudes of the fragment trajectories, can be obtained by interpolation in Table 9.

The heights  $h$  are given in Table 12 computed by means of reference heights  $h_r$  and by means of Fig. 2.

The straight line trajectories were computed for fragments Nos. 5, 6, 8, 9, 11, 13, 14, 15, 16, and 17. The curved trajectories could be detected for the main trajectory No. 1, and for fragments Nos. 2, 3, 4, 7, 10, and 12.

Fig. 3 is very useful and clearly represents the vertical projection of all observed trajectories on the ground. It is necessary to point out that the scale perpendicular to the reference trajectory is much greater than the scale along it. Therefore the curvature and inclination of individual trajectories in Fig. 3 are much greater than in reality. In Fig. 3 the places of meteorite falls are also plotted, as will be given in Section 2.3.

### 1.11 The separation and end points

The points of separation of individual fragments were determined as the intersections of the fragment's trajectory with the main (or parent fragment) trajectory. The geographical longitudes and the heights of the separation points are listed in Table 14.

The end points of the luminous trajectories were directly measured on the Prčice plates and correspond to the absolute limiting magnitude (for the distance of 100 km) of the photographed trails of  $-3^m$ . The geographical longitudes and heights of the end points are given in Table 14.

Table 14

Separation ( $B$ ) and end points ( $E$ ). Diameter of trajectories ( $d$ )

Trail No.	Separated from trail No.	$\lambda_B$	$h_B$ [km]	$\lambda_E$	$h_E$ [km]	$d$ [m]
1		$15^{\circ}20'8''$	97.8	$14^{\circ}11'4''$	13.3	80 38.0*) 26.7
2	1	$14^{\circ}23'6''$	27.9	[ $14^{\circ}15'7''$	18.5]	22.3
3	1	$14^{\circ}27'2''$	32.2	[ $14^{\circ}18'4''$	21.7]	17.5
4	1	$14^{\circ}27'2''$	32.2	[ $14^{\circ}18'4''$	21.7]	15.5
5	1	$14^{\circ}23'6''$	27.9	$14^{\circ}20'6''$	24.2	11.7
6	1	$14^{\circ}21'2''$	25.0	$14^{\circ}19'5''$	23.0	6.8
7	1	$14^{\circ}19'8''$	23.3	[ $14^{\circ}17'8''$	21.0]	17.0
8	3	[ $14^{\circ}22'2''$	26.2]	$14^{\circ}20'0''$	23.6	8.9
9	2	$14^{\circ}21'3''$	25.2	$14^{\circ}20'3''$	23.9	9.4
10	12	$14^{\circ}28'5''$	33.7	$14^{\circ}24'0''$	28.3	12.7
11	12	$14^{\circ}26'4''$	31.4	$14^{\circ}23'7''$	28.0	14.2
12	1	$14^{\circ}34'3''$	40.7	$14^{\circ}23'8''$	28.2	14.5
13	1	$14^{\circ}32'2''$	38.1	$14^{\circ}26'2''$	31.0	10.9
14	1	$14^{\circ}34'3''$	40.7	$14^{\circ}28'3''$	33.6	14.0
15	1	$14^{\circ}33'8''$	40.2	$14^{\circ}27'1''$	31.9	10.6
16	1	$14^{\circ}37'1''$	44.0	$14^{\circ}28'4''$	33.7	11.1
17	1	$14^{\circ}27'2''$	32.2	$14^{\circ}25'9''$	30.6	7.6

\*) diameters of trajectory No. 1 are in the given sequence: maximal, before the first separation and at the end of photographed trail (before the separation of trail No. 7). Diameters of other trails were measured near the separation point.

Trajectories Nos. 1, 2, 3, 4, and 7 leave plate P 1927 at a height of 22.2 km as the lowest limit of our photographic records. The height of the end of trajectory No. 7 was only estimated using the light curve. It was assumed that half the trajectory was photographed.

Trails Nos. 3 and 4 could be distinguished one from the another at height intervals of 28 to 25 km only. They were open to the measurement in the other parts as one brighter trail, which ends almost at the edge of plate P 1927. Therefore the end for both the trails were chosen adding 0.5 km to the height of the last exposed trail.

The height of the end of trajectory No. 2 was estimated only roughly from the light curve. About 60 p. c. seems to be exposed on plate P 1927 and 40 p. c. remains from the edge of the plate to the end.

The end height of main trajectory No. 1 was determined by the combination of the 19 best estimations by visual observers together with the vertical projection of the trajectory obtained from photographs. (See Section 1.12.)

The diameters of the trajectories  $d$  are given in Table 14. These diameters are measured in metres of the real trajectory. The measurements were made near to the separation point of each fragment. The measured diameters (widths) of the apparent trails on the plate are transformed to the real diameters of the fragment trajectories. The diameter of main trajectory No. 1 was measured at three different points, at the point of maximum diameter (80 m), at the point before the first separation, and at the point at the end of the exposed trajectory (before the separation of fragment No. 7).

The diameter of individual trajectories gives not only the dimensions of the region of luminous gas but also relative data about the brightness of individual fragments. A more detailed study of the brightness of individual fragments and especially of regular pulsations, which are present at some fragment trails, will be published later in a paper of this series.

### 1.12 The beginning and end point of the main trajectory

The beginning point of the main trajectory was determined directly from the double-station photographs. According to the rapid increase of the brightness, the beginning was computed very precisely. Its geographical longitude  $\lambda_B$  and height  $h_B$  was

$$\lambda_B = 15^{\circ}20'45'' \quad h_B = 97.8 \text{ km}.$$

The absolute limiting magnitude which corresponds to the beginning was  $-0.6^m$  as will be shown in detail in Section 1.14.

The approximate inclination of the meteorite trajectory to the horizontal plane of the Ondřejov station was  $43^{\circ}$ .

The end point of the main trajectory was off our plates. We must use the combination of visual determinations of this point together with the photographic trajectory. The precision of visual determinations of the direction to the point of the end is small and the trajectory of the meteorite can be represented as a straight line only.

In Fig. 5 the geographical positions of individual casual observers are plotted and the directions which these observers pointed out to us as the observed direction of the end. All these data were obtained by personal

examination of the observers by us directly in the places of observation. All the observations were acquired within 14 days of the meteorite passage. The main attention was directed to the end point at the examination of these casual observers, because we knew that this point was not exposed on our photographs. Altogether 77 observations were acquired by personal examination (we received more than 800 letters about the meteorite fall). The observations of greatest quality were chosen for the determination of the end point. The quality can be proved by such data from the same observer which we can check from our photographs. Thus 19 observations were used and they are plotted in Fig. 5.

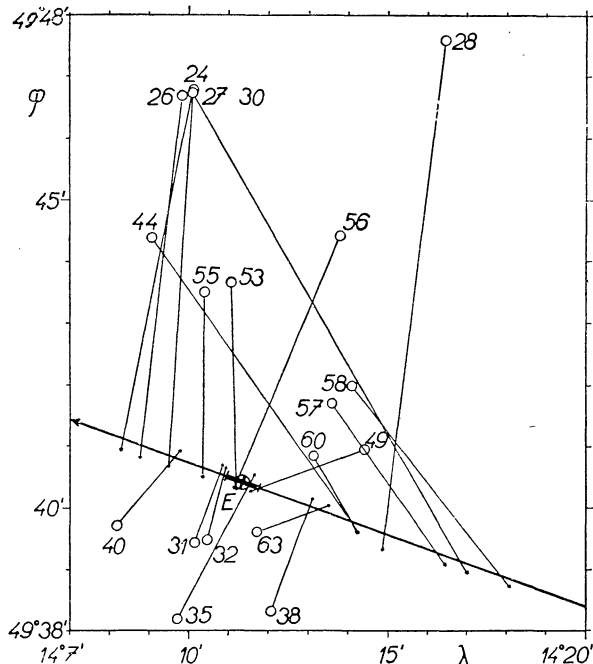


Fig. 5. Determination of the end of the luminous trajectory of the main body using the combination of visual observations with the photographic trajectory. The weighted mean point  $E$  from all intersections was used as the most probable end-point with the given mean error.

Details of the visual observations and of the sound phenomena accompanying the meteorite fall will be published in a later paper of this series.

The given observations of the end point of the main trajectory yield intersections with the photographic trajectory. As the most probable end point the weighted mean from all 19 intersections was taken. The weights of individual intersections were determined according to the angle between the direction to the end and the direction of the trajectory, and according to the distance of the intersection from the observational place. The resulting point of the end of the light trajectory has the following coordinates

$$\lambda_E = 14^\circ 11' \cdot 4 \pm 0' \cdot 4 \quad h_E = 13 \cdot 3 \pm 0 \cdot 5 \text{ km}$$

### 1.13 Double-station fragment No. 15

The heights of Table 12 for fragment No. 15 are only the one-station heights determined by the method of Sections 1.9 and 1.10. But this fragment is the only one

for which the double-station heights are available. The double-station heights can be compared with the heights of Table 12. This fragment has the greatest height difference according to the main trajectory, which is the reason that it was also photographed from Ondřejov. This means that residuals of directly observed heights for this fragment from the heights of Table 12 are the greatest possible for all fragments. If there were some greater differences in heights, such fragments ought to be photographed on the Ondřejov plates. The residuals and thus the maximal possible deviations in height for all fragments are given in Table 15. These residuals are not very great and do not exceed 200 m at the end of the fragment trajectory.

Table 15  
The residuals  $\Delta h$  for trajectory No. 15

$h_{obs}$ [km]	$h_{sm}$ [km]	$\Delta h$ [km]
37.005	37.134	-0.129
36.092	36.231	-0.139
34.883	35.036	-0.153
32.063	32.248	-0.185

$h_{obs}$  height directly from the double-station plate  
 $h_{sm}$  height assumed from the main trajectory (these heights are used for all one-station fragments).

### 1.14 Light curve of the main trajectory

Three quite independent sorts of measurements are available for the construction of the light curve of the falling meteorite.

a) The Ondřejov plates 1924 and 1926, for which the "density" curve can be constructed by means of star trails up to the point corresponding to  $-8^m$  (absolute) of the meteorite trajectory (unguided plates). Additional plates P 1922 and P 1927 were used for the end of the trajectory.

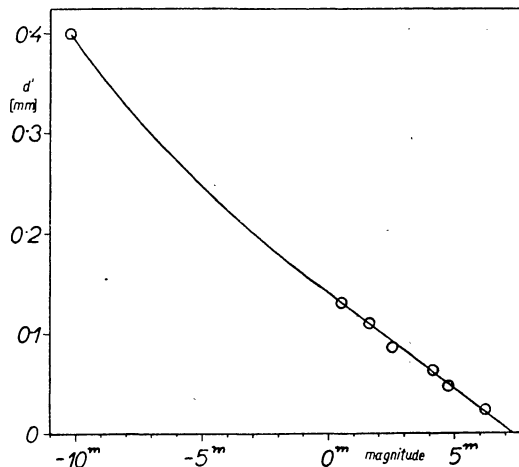


Fig. 6. "Density" curve for plates 1924 and 1926. The value  $d'$  is the apparent diameter (width) of the trail on the plate in mm. Six points on the right refer to star images, the point in the left upper corner corresponds to the maximum light of the meteorite determined photoelectrically. The magnitudes are apparent and for the trailing velocity of stars of 0.01 mm/sec.

b) Visual and photoelectric measurement of the maximum brightness.

c) Indirect photographic determination of the total illumination from photograph of a building on plate G 891.

The "density" curve is plotted in Fig. 6 for plates 1924 and 1926. The measurement of the widths of stellar trails were used for construction of Fig. 6, where the widths are plotted against visual magnitudes of corresponding stars. This star magnitude is corrected for a standard trailing velocity on plates equal to 0.01 mm/sec.

The maximum brightness of the meteorite light was estimated visually by the author using the illumination of the wall of his living room. This illumination was visually compared with the television screen, which the author was watching at the time of the meteorite's passage. The brightness of the television screen was a little less and was increased immediately after the meteorite passage to be roughly the same as the illumination of the wall. Then the brightness of the screen was measured by photoelectric exposuremeter. The result of these estimations and measurements yielded the maximum illumina-

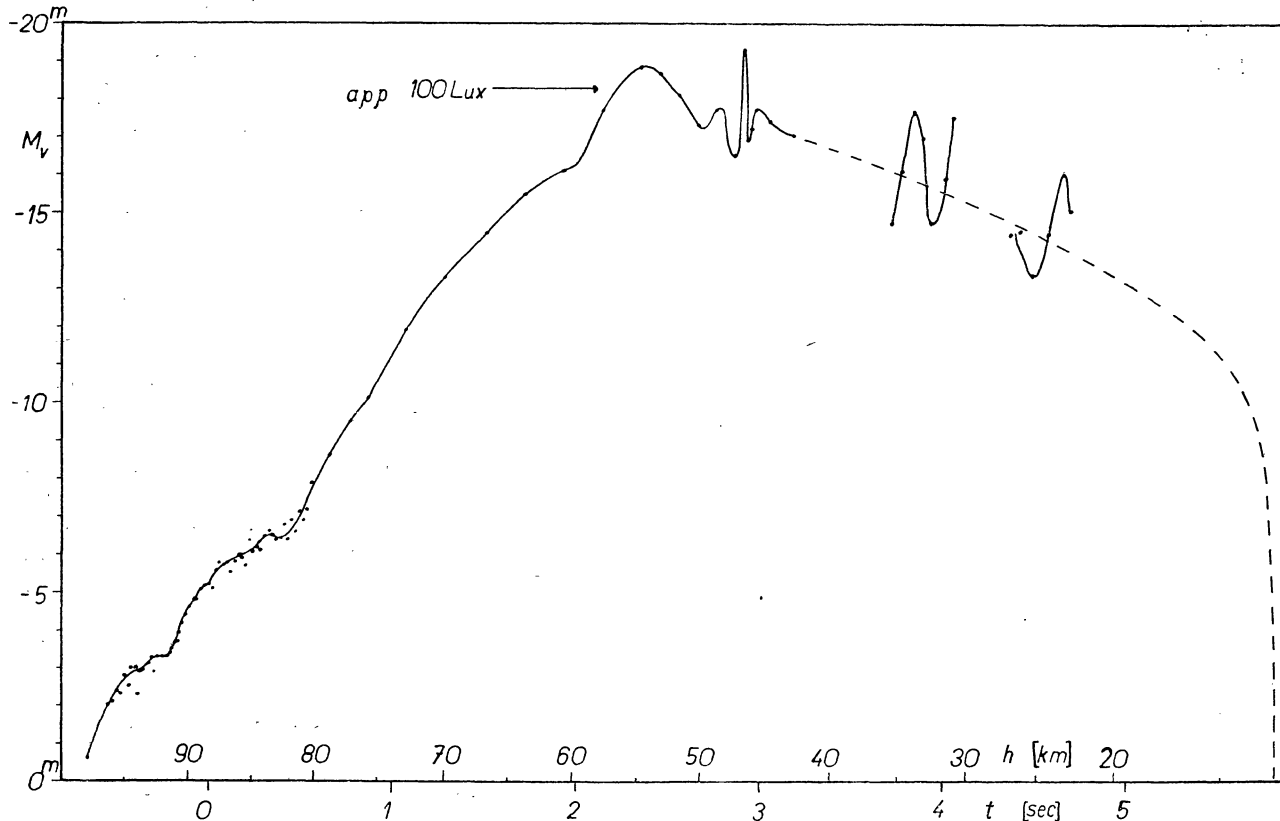


Fig. 7. Light curve of the fireball. The level 100 lux is the apparent illumination at the Ondřejov Observatory. The dashed line is the used schematic light curve.

The magnitudes of individual points on the meteorite trajectory are then determined by the widths of the meteorite trajectory and by reducing these measured widths by means of Fig. 6 to the magnitude system of trailing velocity 0.01 mm/sec. These magnitudes must be corrected for the different trailing velocities of the meteorite and stars (the reciprocity law was used), and for the standard distance of 100 km. These magnitudes are called absolute magnitudes  $M_v$  and are plotted in Fig. 7 as a function of time  $t$  and height  $h$ . More details of the method of reducing the plates to absolute magnitudes of meteors are in paper [1].

The "density" curve is constructed only to the point, which corresponds in the system of absolute magnitudes to  $-8^m$ , using the star trails. The further course of the "density" curve to greater magnitudes was obtained by interpolation between the beginning part of the "density" curve and the value measured for the maximum of meteorite brightness, which is assumed to be at the point of maximum width of the meteorite trajectory.

tion from meteorite of 100 lux, that is of  $-19.2^m$ . This value was used for the construction of the density curve of plate 1926, on which the point of maximum brightness was photographed.

The widths of the meteorite trail were considered as having only photometric significance. But the width of the meteorite trail in the brighter parts of its trajectory represents the real diameter of the luminous trajectory. This is the reason why the "density" curves do not have the typical shape at greater magnitudes, where the overexposure ought to be present. On the other hand, it is possible to suppose that the real diameter of the trajectory increases with increasing brightness. It was possible to determine the ratio of this increase using just the visual-photoelectric measurement of the maximum brightness.

A good check of the visual-photoelectric measurement was possible using an image of the observatory building photographed on plate G 891. The exposure of the building was caused by meteorite light only. Photoelectric measurements of the density of the building image

determined that it was 2 to 3 times overexposed. The normal exposure at the used sensitivity of plates 21/10 Din and at the used focal ratio 1 : 4.5 requires about the total illumination of 50 lux. sec. The total illumination of the building is thus estimated 100 to 150 lux. sec. The integral of the light curve of apparent magnitudes (no correction for the standard distance is used) yields the total illumination of 120 lux. sec, which is a surprising agreement. The light curve is dependent on the maximum value of brightness. Thus the result of integration the light curve of apparent magnitudes proves the visual-photoelectric estimation of the maximum brightness as correct. The increasing branch of the light curve of the meteorite trajectory was thus obtained quite precisely, though the brightnesses are very high.

The decreasing branch of the light curve could be determined only schematically. Plates P 1922 and P 1927 do not contain the point of maximal brightness and the "density" curves must be extrapolated. This extrapolation was effected using the known course of the "density" curve for plate 1926. The measurements of this plate show amplitudes of the light curve of some magnitudes. The decreasing branch of the light curve was used only schematically as it is plotted by the dashed line in Fig. 7. This "dashed" light curve was used in some further calculations.

The total amount of the light energy which was radiated by the fireball is given by the integral of the light curve of absolute magnitudes. (Fig. 7.)

$$E = 2.26 \times 10^7 [M_v = 0 \Rightarrow I = 1] = 0.98 \times 10^{17} [\text{erg}]$$

This value is rather less than in paper [7], where it was determined by simply multiplying the maximum brightness with its equivalent duration. The equivalent duration was only roughly estimated in paper [7] and is 70 p. c. over the accurate value.

### 1.15 The original velocity, radiant, and mass

The influence of the earth atmosphere must be considered if one wishes to know the original velocity and radiant for the orbit computation. The following dependences of the velocity  $v$ , right ascension of the radiant  $\alpha_R$ , and declination of the radiant  $\delta_R$ , on the height (and thus on the air density) were assumed

$$(17) \quad \begin{aligned} v &= v_\infty + c_v e^{-bh} \\ \alpha_R &= \alpha_{R,\infty} + c_\alpha e^{-bh} \\ \delta_R &= \delta_{R,\infty} + c_\delta e^{-bh} \end{aligned}$$

$$(18) \quad c_v = -\frac{\Gamma A v_\infty m_\infty^{-1/3} \rho_0}{b \cos z_R}$$

The result is the same if we use the quantity  $v^2$  instead of  $v$ , because the changes in velocities are relatively small; then formula (18) must be multiplied by  $2v_\infty$ .

The observed velocities and radiants for different heights were used in formulas (17) from Tables 7 and 2. The computation was made by the least square method, which, in this case, goes to the transcendental equations [2]. The results of the least square solution are given in Table 16.

The original velocity was determined from the 6 first measurements of the mean velocity of Table 7 at heights of 88.6, 76.3 (twice), 63.8, 53.0, and 50.2 km. Each mean velocity was weighted according to its mean error.

The first four values from Table 2 were used for the determination of the original radiant (the parts of trajectory 4, 6<sub>1</sub>, 6<sub>2</sub>, 6<sub>3</sub> at heights of 82.9, 74.5, 58.2, and 44.3 km). The weights of individual values were in this case chosen all equal to 1.

Table 16  
The original velocity and radiant  
(least square solution of (17))

	$v$	$\alpha_R$	$\delta_R$
$b \text{ km}^{-1}$	0.080	0.038	0.054
$c$	$17.6 \pm 0.7 \text{ km/sec}$	$48' \pm 5'$	$43'.5 \pm 1'.2$
$v_\infty, \alpha_{R,\infty}, \delta_{R,\infty}$	$20.886 \text{ km/sec}$ $\pm 0.005$	$189^\circ 36' 55'' \pm 33''$ apparent position	$20^\circ 38' 56'' \pm 4''$

The determination of the mean errors of the resulting values is a complicated problem in the case of transcendental normal equations. Therefore the mean errors of the mean values were determined on the assumption that  $e^{-bh}$  is the independent variable on the whole. The resulting mean error of  $v_\infty$  is of the same order as the mean errors of individual velocity determinations. Therefore it is evident that the simplification has no substantial influence on the determined mean errors.

The individual values of velocities are given in Fig. 8. The dependence determined by the least square method is also plotted in this figure.

The preliminary orbit was published in paper [8]. This orbit was determined from preliminary values of  $v_\infty$ ,  $\alpha_{R,\infty}$ ,  $\delta_{R,\infty}$ , which were derived from plates 1924 and

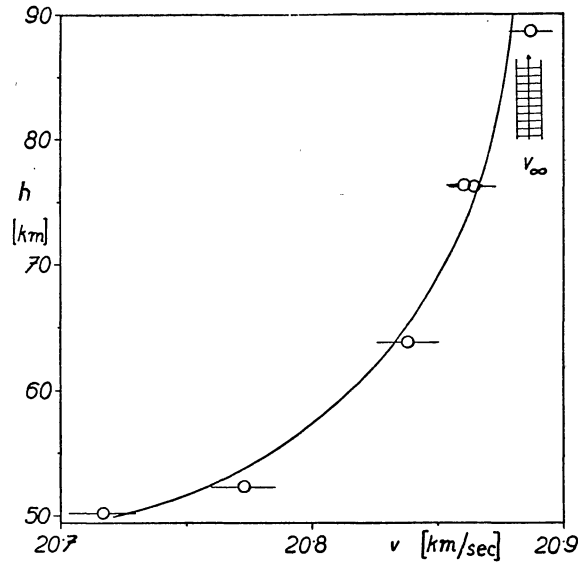


Fig. 8. Observed velocities  $v$  with their mean errors as the function of height  $h$  were used for the determination of the original velocity  $v_\infty$ .

P 1924 of the trajectory beginning. The definitive values of  $v_\infty$ ,  $\alpha_{R_\infty}$  differ from the preliminary ones only by small differences ( $v_\infty$  0.046 km/sec,  $\alpha_{R_\infty}$  33"). The definitive  $\alpha_{R_\infty}$  differs from the preliminary one by a greater value 7'48" as a consequence of a numerical error in the preliminary calculations.

The value  $c_v$ , which results from the least square solution of equations (17) can be used for the calculation of the original mass of the meteorite. Formula (18) determines then the original mass, if we assume the drag coefficient  $I'$  to be known. The shape coefficient  $A$  was taken 0.525 for a spherical shape of 3.5 gr/cm<sup>3</sup> density. The drag coefficient was given different values and thus different original masses were calculated from  $c_v$ :

$$\begin{array}{ll} I = 0.5 & m_\infty = 0.7 \text{ ton} \\ I = 0.7 & m_\infty = 2 \text{ tons} \\ I = 1.0 & m_\infty = 5 \text{ tons} \end{array}$$

### 1.16 The orbit

The orbit was computed from values  $v_\infty$ ,  $\alpha_{R_\infty}$ ,  $\delta_{R_\infty}$  of the preceding chapter. The assumption was used that the descending node of the orbit is in the same place and at the same time as was the Earth at the moment of the meteorite passage. But this supposition has only a small influence on the resulting elements and we can take the orbit of Table 17 as the definitive one. The cause of the deviation from the preliminary orbit is given in Section 1.15.

Table 17  
The orbit

$t$	UT	Apr. 7 81274
$\alpha_{R_\infty}$	app.	189°36'55" ± 33"
$\delta_{R_\infty}$		+ 20°38'56" ± 4"
$v_\infty$	km/sec	20.886 ± 0.005
$\alpha_G$	1950.0	191°31'06" ± 33"
$\delta_G$		+ 17°41'39" ± 4"
$v_G$	km/sec	17.450 ± 0.006
$L_H$	1950.0	131°38'38" ± 25"
$B_H$		+ 9°30'05" ± 12"
$v_H$	km/sec	37.475 ± 0.004
$a$	a. u.	2.424 ± 0.002
$e$		0.6742 ± 0.0005
$q$	a. u.	0.7899 ± 0.0012
$\omega$		241°34'58" ± 11"
$\Omega$	1950.0	17°06'38"
$i$		10°25'28" ± 15"
$\pi$		258°41'36" ± 11"

The computation of the orbit was effected by progressive subtraction of all effects: diurnal abberation, zenith attraction and the velocity of the Earth in its orbit. The resulting heliocentric radiant and velocity determine the orbital elements.

Each value of Table 17 is given with its mean error, which was determined from mean errors of independent values  $v_\infty$ ,  $\alpha_{R_\infty}$ ,  $\delta_{R_\infty}$ .

### 2. Finds of meteorites

#### 2.1 Actions in connection with meteorite finds

This section contains a brief discription of all actions in connection with the meteorite finds. A more detailed description will be published later.

The members of the Interplanetary Matter Department of the Astronomical Institute in Ondřejov organized all

the necessary work connected with the search for meteorites. Just after the meteorite passage the rough trajectory was determined from photographs. This enabled us to choose the region in which it was necessary to obtain the visual observation of the end of the main trajectory. We obtained 77 visual observations in this region during the first 14 days after the meteorite passage as was mentioned in Section 1.12. This region contained the probable places of the meteorite falls. Thus we combined the action of obtaining visual observations with the action of announcement to the inhabitants that it is possible to find meteorites. We used the village broadcastings, personal propaganda, and publications on the village notice boards.

The stony meteorite "Luhy" was obtained by us on 20th April, 1959. This meteorite weighing 4.48 kg was found by V. Vršeký on 9th April when he was working in his field. We concentrated on searching for further meteorites only after 20th April.

We made a systematic search of the region denoted a) in Fig. 4, in an attempt to find a larger meteorite. In this work we obtained the help of the local inhabitants. The entire region in which we searched was covered by young forest. This search was continued from 22nd to 30th April with a negative result.

We obtained the second meteorite on 9th June 1959. This meteorite, called "Velká 1", weighing 0.80 kg was found by A. Plavec while working in the field on 24th April. He also found on the same day another meteorite, "Velká 2", in the vicinity of the first one, but left this second piece in the place, where it was found. This meteorite was not found again, when we and the finder searched on 9th June (during our visit when we stated that the stone which was found was the meteorite). The weight of the second Velká meteorite was said to be 'greater but surely not twice the weight of "Velká 1" meteorite'. The shape 'was more spherical than in the case of "Velká 1" and one side was deformed in three drops'.

The Velká 1 meteorite was broken by the finder into 3 pieces with a hammer. The smallest piece was lost (30 gr only) by the finder.

The expedition of ten observatory staff was arranged from 20th July to 5th August, 1959, with the aim to search the region b) (Fig. 4). About one half of this region, which was covered by stubble-fields after the harvest, can be searched. The other half of this region was covered by clover, meadows and partly by woods. Our attention was concentrated on the vertical projection of trajectory No. 7, which was traced by means of wooden stakes. The result of this search was negative.

This expedition acquainted the inhabitants of the region with the possibility of meteorite finds, and with the appearance of meteorites by means of the found meteorite "Velká 1".

We obtained the meteorite "Hojšín" on 19th August, 1959. This meteorite weighing 0.42 kg was found on 15th Aug., by M. Kramešová in a crop of clover only 12 m from the trajectory of fragment 7, which was staked out on both sides of the field.

We obtained the meteorite called "Dražkov" on 25th Aug., 1959. This meteorite was found on the previous day by V. Vácha, a 13 year old schoolboy. The weight of this meteorite is 104 gr.

Though we kept the possibility of further finds in the attention of the inhabitants in the "meteorite" region during autumn 1959 and spring 1960, no further meteorites were found.

We ascertained in early spring 1960, that we had considered the meteorite "Luhy" as the main body only by mistake. The biggest meteorite belonging to the main trajectory No. 1 ought to weigh about 100 kg. This body remains to be found [9].

We organized a further expedition of 7 observatory staff to the region c) (Fig. 4) from 5th April to 20th April and from 2nd May to 7th May, 1960. Region c) is contiguous with regions a). This region c) was very unfavourable for finding the body, though its linear dimensions must be about 40 cm. Almost the whole region was covered by young forest, which makes the search very difficult. Visibility was limited in thickets to 1 or 2 m only. There were places which were impossible to search at all. A systematic search was possible only 30 to 50 m from the trajectory staked out, because the expedition was not numerous. The result was negative. But it is not excluded that in the future the main meteorite will be found by woodmen.

We staked out and partly also searched in the same season fragment trajectories Nos. 11, 12, 5, 6, and 9. We acquainted the inhabitants with the regions of possible finds of individual fragments. One of these regions includes the village Dražkov.

## 2.2 Some data about meteorites

The meteorites are chondrites. The detailed data about chemical and mineralogical composition will be published in the second paper of this series.

Meteorites Luhy, Velká 1, and Dražkov are individual pieces almost all covered by black primary crust. Only small places on these meteorites are without any crust or with a faint secondary crust. The thickness of the crust measured on the Velká meteorite varies between 0.29 mm to 0.03 mm (at grains of NiFe). The most frequent thickness of the crust is 0.29 mm and 0.18 mm. Other thicknesses are rare. Meteorite Velká 2 was also an individual piece with the primary crust over the whole surface according to the data of the finder.

The Hojšín meteorite is only a fragment of the individual piece belonging to the photographed trajectory No. 7. A great part of its surface is without any crust (fracture side). Because this meteorite was found 4 months after its fall, the fracture side was weathered. At one edge of the fracture side the primary crust, which is bent over the edge, is evident. This is of course evidence of the crack on the surface of the original whole individual piece. This crack must originate at the very end of the luminous trajectory, just before the formation of the solid crust. The fracture was then finished during the dark trajectory of the meteorite, when the solid crust cannot be formed. Thus the fracture remained without the crust. It is possible to estimate the weight of the whole individual piece belonging to trajectory No. 7 only roughly. It is between 0.6 and 0.8 kg, that is about one half is the Hojšín meteorite.

The place of fall of the second part of the individual piece belonging to trajectory No. 7 can be relatively far

from the place of the Hojšín meteorite. This is strongly dependent on the shape of the body, especially if the fracture was finished just after the end of the light trajectory (Section 3.2). The immediate neighbourhood of the Hojšín meteorite was completely searched without results.

The densities of the meteorites were roughly estimated to be about  $\rho_M$  3.5 gr/cm<sup>3</sup>. Further measurements of greater precision will be given in the following paper of this series, and yield a little higher value of density.

The head cross-sections will be used in this paper for the computation of the "dark-flight" distance. These cross-sections were determined for individual meteorites as follows (provisional values)

$$\begin{aligned} \text{Luhy} &= 144 \text{ cm}^2 \\ \text{Velká 1} &= 38.5 \text{ cm}^2 \\ \text{Hojšín} &= 30.5 \text{ cm}^2 \\ \text{Dražkov} &= 8.65 \text{ cm}^2 \end{aligned}$$

It is hardly possible to determine the orientation in flight of the last three meteorites without aerodynamical measurements. These data will be given more accurately in some further papers of this series.

## 2.3 Places of the falls

The Luhy meteorite fell in a rye-field with young corn. It penetrated to a depth of 20 cm in the arable soil and rebounded 30 cm from this point, where it was found just on the surface. The soil partially fell in and the resulting pit was only 8 cm deep. The place of the Luhy meteorite fall is plotted in Fig. 9 with the meteorite in position given by the finder. Fig. 9 was constructed using direct and photographic measurements of the place.

A regular symmetric half egg-shaped pit appeared after the loose soil had been scraped up. The profile of the pit is plotted in Fig. 9. It was possible to determine accurately the orientation of the Luhy meteorite at the penetration into the soil. This orientation was marked on the head part of the meteorite alone. The head part was covered by the cleaving soil. It was possible to put the meteorite in such a position in which just the whole "soil" part was visible and the whole clear part was invisible. This is the position, which the meteorite occupied on penetrating into the soil, and probably also during the preceding "dark" trajectory. This orientation corresponds well with stable non-rotational flight.

Meteorites Velká 1 and Velká 2 fell on arable soil with a relatively high content of sand. They were sunk only 2 or 3 cm in the soil according to the data of the finder. The precise places of fall could not be found again by us when we came to the places more than one month after the find. But there were many objects suitable for accurate location (the road, trees, a path in the field) in the vicinity of the meteorite falls. Therefore the places which were estimated by the finder could hardly be farther than 10 m from the real places.

The Hojšín meteorite was found in a clover field at the second crop. This meteorite lay directly on the surface without any disturbance of the ground being visible. In contrast with the above cases, this field was full of stones with some rocks jutting out of the soil. Because of the

Table 18  
The found meteorites

Meteorite	Weight $m_E$ [kg]	$\lambda$	$\varphi$	$h$ [m]	$\lambda_r$	$D$ [m]
Luhý	4.48*)	14 10 51.24	49 40 19.70	425	14 11 00.40	-527
Velká 1	0.80*)	14 14 49.1	49 39 32.9	310	14 14 53.34	-246
Velká 2	0.80-1.5	14 14 51.3	49 39 33.0	311	14 14 55.25	-228
Hojšín	0.42	14 16 01.04	49 39 03.34	330	14 16 11.63	-606
Dražkov	0.104	14 17 15.10	49 39 19.69	351	14 17 08.46	+377

\*) Weights given in this paper hold for the whole individual pieces; the lost material is estimated and added to the measured value.

fact that the meteorite was in this field during the first crop of the clover, there is a possibility that the stone was transported by a raking-machine about 15 to 20 m northwards. The place of find is suitable for this theory because the meteorite was found below the south edge of a great stone (top of the rock).

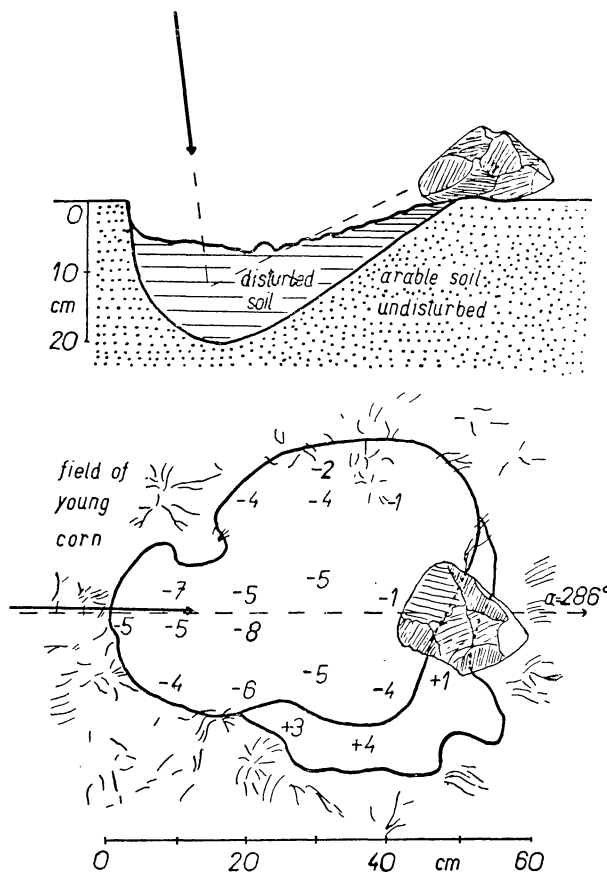


Fig. 9. Ground-plan (below) and the profil (above) of the fall place of the Luhý meteorite. The meteorite is in that position in which it was found. The numbers mean the depression or elevation according to the surface of the field. The azimuth  $a = 286^\circ$  is the measured one. The direction of the meteorite fall plotted by full arrow was calculated theoretically from Eqs. (23), (24) and corresponds well with the shape and position of the pit.

The Dražkov meteorite fell at the edge of a forest on the moss not far from a path. This meteorite lay directly on the surface. The outline of the meteorite was only traced in the moss.

The rectangular coordinates of the Křovák geodetical system [6] were used to measure the places of fall of the meteorites. A Wild theodolite was used. The coordinates of trigonometrical points were used. These measured rectangular coordinates were transferred to the corrected geographical coordinates on the Bessel ellipsoid (they were corrected for shifting and turning the local geodetical system against the system related to the stars). Some further details were given in Section 1.4. The resulting geographical coordinates of the places of meteorite falls are listed in Table 18 with the heights of these places above sea-level. \*) The perpendicular distances  $D$  of the places of falls from the projection of the reference trajectory to the ground are also given in Table 18 (section 1.8). The sign + means the deviation to the right (north) and the sign - means the deviation to the left (south) of the reference trajectory.

#### 2.4 The dispersion "ellipse"

It is usual to speak about the dispersion "ellipse" of a multiple meteoritic fall. Even if this term is not suitable, I will use it.

The minor axis of this ellipse is given by the relative positions of the found meteorites. The Dražkov meteorite is the fragment which deviated farthest to the right and the Hojšín meteorite is the fragment which deviated farthest to the left (Fig. 3.). The distance between these two meteorites in the direction perpendicular to the motion of the main body 983 m is also about the minor axis of the dispersion ellipse.

The major axis of the ellipse will be certainly greater than 8 km, that is the distance between the Luhý and the Dražkov meteorites. It is possible to take this major axis as 15 to 20 km according to the computed places of fall of the main not-found body. However, the dispersion of meteorites along the trajectory is about 20 times greater than across it.

It is better in future to use the terms the dispersion along the trajectory and the dispersion across the trajectory rather than the terms minor and major axis of the dispersion ellipse.

\*) The geographical coordinates given for the Luhý meteorite in the preliminary paper [6] are not correct due to numerical errors in the computation.

### 3. The relations between the photographed trajectories and places of meteorite falls

#### 3.1 The velocity at the end of the luminous trajectory

The velocity at the end of the luminous trajectory (more exactly at the end of the photographed trajectory in our case) is one of the most important values, which determine mainly  $\Lambda$  and thus also the masses of the not found meteorites. The drag coefficient  $\Gamma$  is less influenced by the value  $v_E$  but for the determination of  $\Gamma$  this velocity is also important.

We shall try to determine the value  $v_E$  directly from the measurements of velocities of fragment No. 15. We use the direct measured velocities of Table 8. We suppose that the velocity follows the dependence

$$(19) \quad v^2 = v_\infty^2 + C_Q$$

$$(20) \quad C = -\frac{2\Gamma A v_\infty^2 m_\infty^{-1/3}}{b \cos z_R}$$

which is the first approximation for the case of constant  $\Gamma, \Lambda$ . The value  $v_\infty$  in these relations must be considered as the hypothetical original velocity, which the body would have on entering the atmosphere as an independent body. The velocity  $v_\infty$  for a fragment trajectory is always greater than for the main body.

The method of least squares together with the numerical data of Table 8 used in the formula (19) will yield the following results:

$$C = -(3.0 \pm 1.1) \times 10^{17} \text{ (cgs.)}, \\ v_\infty = 20.9 \pm 1.6 \text{ km/sec}$$

These values yield the velocity  $v_E$  at a height of the end  $h_E$

$$v_E = 10 \pm 7 \text{ km/sec}$$

This value, which corresponds to the point where the meteorite practically ends its evaporation, is determined with relatively great mean error. The condition:  $v_\infty$  of the fragment  $> v_\infty$  of the main body determines the interval of  $v_\infty$  for fragment No. 15 from 20.9 to 22.5 km/sec. The corresponding interval of  $v_E$  is from 10 to 3 km/sec. Thus the most probable value of measured  $v_E$  differs not much from 7 km/sec, which is the theoretical value corresponding to the mean energy of the crystal lattice. This value  $v_E = 7 \text{ km/sec}$  was used in most of the computations of the following sections. It is evident from the results of the following sections that this value of 7 km/sec satisfies the bigger meteorites, but is too small for smaller meteorites. Values about 10 km/sec must result for meteorites of the size of the order of fragment 15.

The velocity at the point of separation of fragment 15 results then from the relation (19) to  $18 \pm 2 \text{ km/sec}$ , which is in agreement with the velocity of the main body at this point. The mass  $m_\infty$  resulting from (20) is then about 700 gr.

We can use another dependence of velocity on the air density

$$(21) \quad \log v = \log v_\infty + B_Q \\ B = \frac{-\Gamma A m^{-1/3} \log e}{b \cos z_R}.$$

These relations hold in the case when no mass is evaporated from the fragment during its flight. Thus the results according to formula (21) are certain upper limits of the velocity  $v_E$ . If we use the values of Table 8 and the method of least squares for (21), we obtain

$$B = -(0.027 \pm 0.010) \times 10^{-6} \text{ (cgs.)}, \\ \log v_\infty = 6.37 \pm 0.06.$$

The velocity at the end then results from these values

$$v_E = 11.4 \pm 3.4 \text{ km/sec}.$$

The velocity at the separation point is then  $18 \pm 3 \text{ km/sec}$ , which corresponds with the velocity of the main body at this point.

We can compare how relations (19) and (21) satisfy the measured values of Table 8. The sum of squares of deviations (calculated minus observed velocity) are then

$$\text{relation (19): } 3.00 \text{ km}^2/\text{sec}^2$$

$$\text{relation (21): } 3.06 \text{ km}^2/\text{sec}^2$$

Both these values are practically the same and it is not possible to say on the basis of measurements only which relation is better.

In Section 3-3 the value of  $v_E = 11.4 \text{ km/sec}$  will also be used for the Dražkov meteorite. The value 7 km/sec is used for bigger meteorites. Both these values can result from relations (19) and (21) for fragment No. 15.

The constant mass  $m$  resulting from (22) is about 100 gr., which is less than the value that results from (20). This is also in agreement, because relation (20) yields the hypothetical original mass only.

#### 3.2 Dark-flight distances

The term "dark-flight" distance  $L$  is used for the distance from the end of the light trajectory to the place of meteorite fall measured in the projection to the horizontal plane. The mass of the meteorite is constant in this part of the meteorite trajectory in contrast with the preceding luminous trajectory. Therefore it is possible to use the classical motion-equations.

A strong wind blew at the time of meteorite passage. It is necessary to introduce its influence into the motion equations. The wind was almost exactly directed in all heights against the azimuth of the meteorite flight. Thus it was sufficient to compute only the vertical and horizontal component of the velocity in the vertical plane of the meteorite trajectory. It holds

$$(23) \quad \frac{dv_e}{dh} = \frac{\Gamma S_Q v(V + v_e)}{v_h}$$

$$(24) \quad \frac{dv_h}{dh} = \frac{\Gamma S_Q v v_h - g}{v_h}$$

where

$$(25) \quad S = \frac{s_E}{m_E}$$

and

$$(26) \quad v^2 = (V + v_e)^2 + v_h^2.$$

The direct solution of these equations is not yet possible in the case of  $V = 0$ . But  $V$  changed with the height

quite irregularly. It is necessary to use a numerical calculation. We start from the components of the velocity  $v_e$  and  $v_h$  at the end point, which are given by the velocity  $v_E$  and by the zenith distance of the radiant. Then the equations (23) (24) can be integrated numerically by step-by-step integration.

This procedure is very laborious and we had to limit our computation to several cases, which were used in the construction of Fig. 12. One point in this Fig. 12 represents the results of the whole numerical solution of equations (23) and (24) with commencing conditions given by the above mentioned velocity components and with the height of the end of the luminous trajectory  $h_E$ . The construction of Fig. 12 was thus performed splitting up the whole dark-flight distance into three components, which depend on different parameters of the problem.

The numerical integration of equations (23) and (24) was performed using a height interval of 0.1 km. The velocity components  $v_e$  and  $v_h$  result as the functions of height. Then the dark-flight distance is given

$$(27) \quad L = \int_{h_s}^{h_E} \frac{v_e}{v_h} dh .$$

This integral was also calculated numerically. All computations were made using normal mechanical computers. We plan to use an electronic computer in future to solve this problem more accurately. Then Fig. 12 will be drawn using hundreds of results, which is not possible in this case.

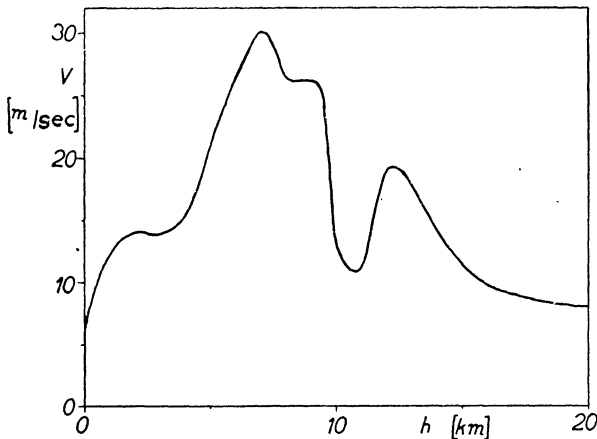


Fig. 10. Component  $V$  of the wind velocity against the azimuth of the meteorite flight determined by direct meteorological measurements.

The drag coefficient is contained in equations (23) and (24). This drag coefficient  $\Gamma$  was taken as the function of the Mach number  $\Gamma = \Gamma(M)$ . This function was chosen for  $M$  greater than 1 using the results of paper [10]. Only the shape of this function was supposed, the level was then determined from Fig. 12 for individual meteorites. A constant drag coefficient  $\Gamma$  was used for  $M$  less than 1 and its value was chosen as 0.52 of the value  $\Gamma$  for  $M = 6$ . The  $\Gamma$  for  $M$  greater than 6 was again assumed to be constant.

The numerical computations of Fig. 12 were performed using the following values of  $\Gamma$ :

$$\begin{array}{lll} \Gamma(6) = 0.77 & \Gamma(3) = 0.79 & \Gamma(2) = 0.84 \\ \Gamma(1.3) = 0.82 & \Gamma(1.1) = 0.61 & \Gamma(0.9) = 0.40 \end{array}$$

The computations were performed for different values of  $\Gamma S$ , because  $\Gamma$  is contained in equations (23) and (24) in the product  $\Gamma S$  only. The numerical values of  $\Gamma S$  in Fig. 12 are referred to the  $\Gamma$  for  $M \geq 6$ . This holds for all values of  $\Gamma$  given in the following sections. The results of the numerical solution of equations (23), (24), and (27) can be used not only for the  $\Gamma(M)$  given above, but also for all values of  $\Gamma$ , for which the  $S$  is chosen so that the product  $\Gamma S$  remains the same.

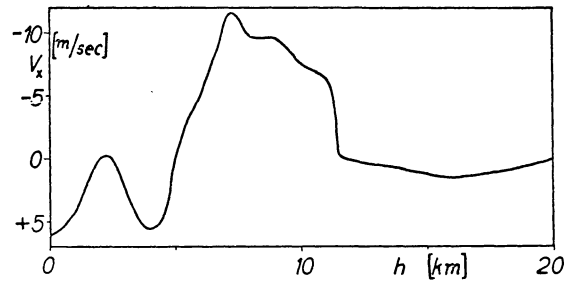


Fig. 11. Component  $V_x$  of the wind velocity perpendicular to the azimuth of the meteorite flight from direct meteorological measurements.

As soon as the values of  $\Gamma$  and  $S$  are measured directly by laboratory experiments some computations of Section 3.3 using Fig. 12 can be made more accurately.

The head cross-section  $s_B$  is contained in equations (23) and (24). This value was measured for individual meteorites as is stated in Section 2.2. The orientation, at which these meteorites penetrate the atmosphere at their dark-flight trajectory, was determined only by rough estimation. This was well possible for the Luhy meteorite, but was very uncertain for the Hojšin meteorite. Only aerodynamical measurements could yield definitive results.

The air density  $\rho$  is contained in equations (23) and (24). The density  $\rho$  was used up to the height of 20 km from direct meteorological measurements of pressure and temperature. The mean variation of density with height was used at greater heights for the spring season and geographical latitude  $+50^\circ$ . The temperature necessary for the determination of the Mach number was used from the same measurements.

The wind component against the azimuth of meteorite flight  $V$  is contained in equations (23) and (24). Direct measurements by meteorological balloons were again used up to a height of 20 km. The wind velocity at greater heights was supposed constant at 8 m/sec, because in all practical cases the velocities of meteorites at these heights are too great to permit observation of any wind velocity effect. The wind velocity component against the azimuth of meteorite flight is plotted in Fig. 10 as a function of the height. The component of the wind velocity perpendicular to this azimuth  $V_x$  is given in Fig. 11. From these figures it is evident that the strong wind blew almost against the direction of the meteorite

and thus caused a substantial shortening of the dark-flight distances. The mean component of the wind velocity perpendicular to the meteorite trajectory at the height interval from 20 km to the ground was  $-0.7 \text{ m/sec}$  only. The influence of the side-wind component was not computed in detail. Approximate computation shows

The results of the numerical solution of equations (23), (24), and (27) are plotted in Fig. 12, where the dark-flight distance is on the  $x$ -axis and the end height of the luminous trajectory on the  $y$ -axis. The parameter  $\Gamma S$  is used for  $M \geq 6$  from which the  $\Gamma$  can be determined for  $M \geq 6$ . Using Fig. 12 the dark-flight distance can be de-

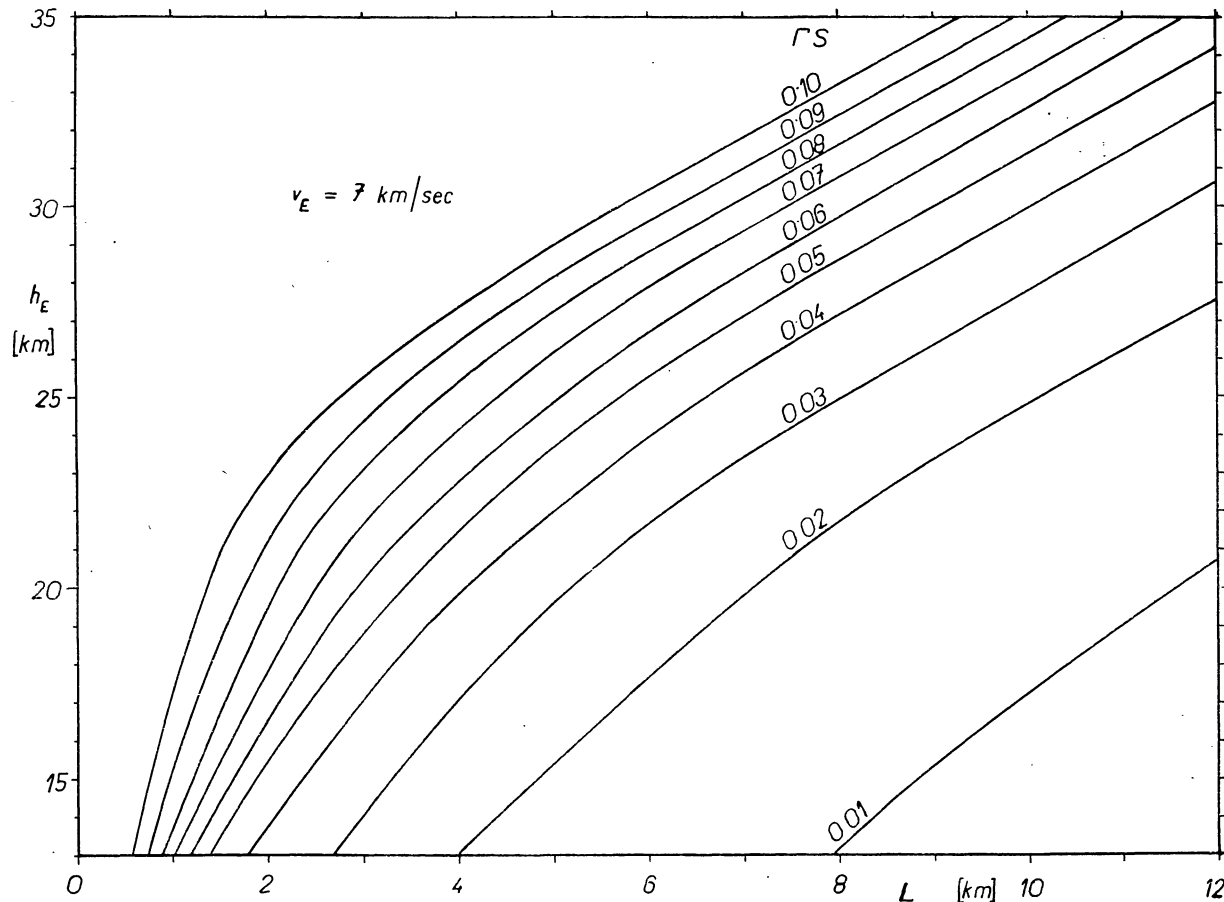


Fig. 12. Dark-flight distances  $L$  as functions of the end heights  $h_E$  of the luminous trajectories calculated from equations (23) and (24). The parameter  $\Gamma S$  represents the shape, density and dimensions of the body. This figure was used for the identification of individual found meteorites with the photographed fragment-trajectories.

that it is possible to reach deviations of some hundreds of meters from the projection of the original trajectory. This corresponds to the deviations of the meteorites from its trajectories as they are given in Table 19.

The computations of equations (23) and (24) start from the value  $v_E$ , that is from the velocity at the end of the luminous trail. The theoretical value 7 km/sec was used throughout the computations. The drawback of such a value is the fact that  $v_E$  at the observed (photographed) end of trajectories can be a function of the brightness of the trail, and thus of the mass of the meteorite. The velocity  $v_E$  for smaller meteorites as for Dražkov can be greater than 10 km/sec. When other velocities than  $v_E = 7 \text{ km/sec}$  were considered in Section 3.3, these velocities had to be transformed to 7 km/sec using equation (21), which holds for  $m = \text{const}$ . This was necessary to permit the use of Fig. 12, which is computed for 7 km/sec only.

terminated and the place of the probable fall of the not found meteorites can be computed, if a rough estimation of  $S$  is possible. The observed dark-flight distances for the found meteorites are given in Table 19.

Further results of the numerical solution of equations (23), (24) are the velocities  $v_s$ , with which the meteorites meet the ground and the zenith distance of their direction at that moment  $z_s$ . The negative sign of  $z_s$  means that the direction is opposite to the original direction of the meteorite trajectory due to the influence of wind. These theoretical values of  $v_s$  and  $z_s$  correspond well with the observed effects for the Luhy meteorite (depth and orientation of the pit; Fig. 9). The theoretical depth computed with  $v_s = 78 \text{ m/sec}$  for a medium hard soil using paper [11] is 21 cm. The values  $v_s$  and  $z_s$  are also given in Table 19 for the found meteorites and can be determined for other values of  $\Gamma S$  from Fig. 14.

The whole calculated trajectory of a dark-flight is plot-

Table 19  
The trajectories corresponding to the individual found meteorites

Meteorite	Trajectory No.	$D_M$ [m]	$S$ [cm <sup>2</sup> /gr]	$A$ [cm <sup>2</sup> /gr <sup>2/3</sup> ]	$v_E$ [km/sec]	$L$ [km]	$\Gamma$	$v_s$ [m/sec]	$z_s$
Luhý	2	- 153	0.032	0.53	7	5.7	0.72	78	- 6.8
Velká 1	3	- 59	0.048	0.45	7	4.2	0.99	58	- 10.8
Hojšín	7	+ 12	0.073	0.54	7	2.0	1.20	42	- 14.0
Dražkov	10	+ 12	0.083	0.39	7	8.2	0.55	59	- 10.6
					11.4	5.9*)	0.68	53	- 11.8

\*)  $L$  is measured from the point, where the velocity of 7 km/sec is reached (Eqs. (21) and (22)).

ted in Fig. 13 in order to demonstrate how rapid is the change of direction in the case of oblique penetration of the body in the atmosphere and how substantial is the influence of the wind.

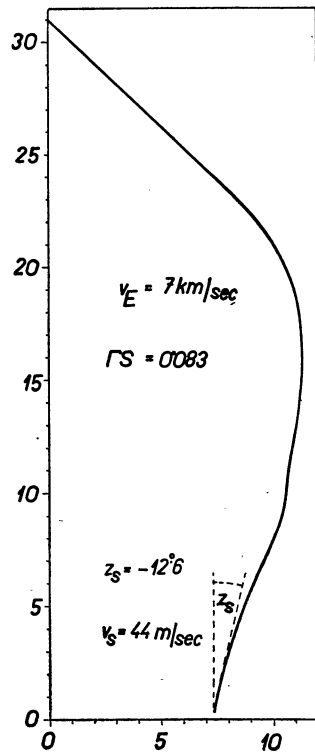


Fig. 13. Theoretical dark-flight trajectory of a meteorite, which is similar to the Dražkov meteorite (solution of (23) and (24)). The effect of wind on the trajectory is very substantial.

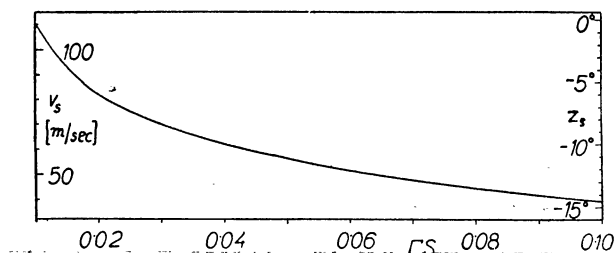


Fig. 14. A meteorite colliding with the earth surface at the velocity  $v_s$  had the zenith distance of its direction at this moment  $z_s$ . Both these values are plotted against  $r_s$  as one curve only.

### 3.3 The identification of meteorites with photographed trajectories

An identification of photographed trajectories with the found meteorites was used in paper [7] for the computation of a series of important data. This identification in paper [7] was carried out on the basis of the vertical projection of trajectories of individual fragments only, and thus it is not correct. The dark-flight distance must be taken as the decisive value. Identification by using the dark-flight distances is more reliable because dispersion of the meteorites along the direction of the meteorite motion is 20 times greater than dispersion across this direction [9].

Identification of meteorites with trajectories as results from the computations of the preceding section is given in Table 19. The observed dark-flight distances  $L$  and the transverse distances  $D_M$  from the extrapolated trajectory of the fragment are given for the found meteorites in Table 19.

The observed dark-flight distances are used in Table 20 for the computation of the drag coefficient  $\Gamma$  at different identifications. Fig. 12 was used for these computations.

Identification of meteorite Luhý with trajectory No. 1, as was determined in paper [7] would mean that the drag coefficient is 3.5. Hence it is evident that the Luhý meteorite belongs to trajectory No. 2. The deviation of 153 m to the left of the extrapolated trajectory was caused by the transverse component of the wind,

Table 20  
 $\Gamma$  for different possible combinations of meteorites and trajectories

Meteorite	Trajectory No.	$L$ [km]	$\Gamma$	$m_B$ [gr]
Luhý	1	0.4	3.5	
	2	5.7	0.72	
Velká 1	2	1.0	$\approx 3$	
	3,4	4.2	0.99	
Dražkov	10	8.2	0.55	160
	13	11.3	0.44	30
Dražkov	10	5.9*)	0.68	710
	13	7.1*)	0.59	160

\*)  $L$  is measured from the point, where the velocity of 7 km/sec is reached (Eqs. (21) and (22)).

which has an average value for this meteorite of about  $-2 \text{ m/sec}$ , or by an inaccuracy of the extrapolation. The preliminary computation of the extrapolated trajectory No. 1 yielded only  $30 \text{ m}$  deviation from the found meteorite Luhy due to a numerical error. This small deviation was the main reason for the wrong identification of the Luhy meteorite with main trajectory No. 1 in paper [7].

Meteorites Velká 1 and Velká 2 correspond to trajectories Nos. 3 and 4 according to the dark-flight distances. It is quite impossible to say on the basis of the dark-flight distances to which of these two trajectories meteorite Velká 1 belongs. The end points of both the trajectories are in the close vicinity, and the meteorites were both found in the close vicinity, too. This corresponds to practically the same mass of both meteorites, which is not in contradiction of the mass estimation of Velká 2 meteorite by the finder (Section 2.1). Thus both the identifications are possible. We use in this paper for the sake of uniformity the identification of Velká 1 meteorite with trajectory No. 3. The reasons for this identification are in the elongated shape of Velká 1 meteorite and the most extensive light-pulsations of trajectory No. 3. On the other hand Velká 2 meteorite had a more symmetrical and spherical form (according to the data of the finder) and trajectory No. 4 is without pulsations at all. Velká 1 meteorite was identified in paper [7] with trajectory No. 2. This wrong identification would require the drag coefficient to be about 3.

The Hojšín meteorite flew farthest to the left of the main trajectory. The identification of this meteorite with trajectory No. 7 cannot be doubtful, because the meteorite was found only  $12 \text{ m}$  from the computed and staked out trajectory. The relatively great value of  $\Gamma = 1.2$  resulting from Fig. 12 must be taken with reserve, because the orientation of the Hojšín meteorite during flight could be determined only very roughly and is not sure.

The Dražkov meteorite flew farthest to the right of the main trajectory. Its identification with trajectories Nos. 10 and 13 is possible. The identification with the trajectory No. 13 was used in paper [7]. It is not possible to be sure of the identification using only the dark-flight distances and vertical projections of trajectories. But the mass  $m_B$  at the separation point of each of these two trajectories may be determined using formulas (19) and (20) and the values  $v_B$ ,  $v_E$ ,  $\varrho_B$ ,  $\varrho_E$ . This mass can be compared with the mass of the Dražkov meteorite. The mass  $m_B$  for trajectory No. 13 is less than the mass of the Dražkov meteorite. This was the reason for the identification of the Dražkov meteorite with trajectory No. 10.

The relatively small value of  $\Gamma$  for the Dražkov meteorite can be explained so that the end velocity ought to be taken as greater than  $7 \text{ km/sec}$ . The value  $v_E = 11.4 \text{ km/sec}$  was also used for the Dražkov meteorite (Section 3.1). The masses at the separation points were computed. Identification in this case is not unique and both the identifications are possible, because the mass  $m_B$  is greater than the mass of the Dražkov meteorite for both identifications.

In both cases, with  $v_E = 7$  and  $11.4 \text{ km/sec}$ , it is possible to say that the identification of the Dražkov

meteorite with trajectory No. 10 is more probable than with trajectory 13.

Identification of the Dražkov meteorite with trajectory 13 was used in paper [7]. This identification was determined on the basis of the vertical projections of the trajectories only. The preliminary computation for trajectory 10 was performed with the straight-line trajectory only, and this projected trajectory No. 10 passed at a much greater distance from the position of the Dražkov meteorite than trajectory No. 13.

The probable places of the not found meteorites as they result from Fig. 12 are given in Fig. 3.

#### 4. The mass of the not found meteorites

##### 4.1 The mass from the trajectory diameter

The diameters of the luminous trajectory were used for the determination of meteorite masses in paper [7]. The wrong identification of trajectories with meteorites can be corrected according to the results of this paper. The dependence of the luminous-trajectory diameter on the meteorite mass is given in Fig. 15, in analogy with Fig. 1 of paper [7], using the correct identification. The masses of all meteorites are then given in Table 21.

It is not quite clear which diameter must be taken from Table 14 for the main trajectory No. 1 for mass determination. There are two possibilities: namely in the point near the last separation and before the first separation, as limits of the mass. The uncertainty of the mass determination of the biggest meteorite is the cause of the uncertainty of the determination of the total mass of all the meteorites which reached the earth surface.

Table 21  
The computed meteorite masses  $m_E$  corresponding to all trajectories

Trajectory No.	$m_E$ trajectory diameter Fig. 15	$m_E$ dynamical (28), (29), (30)	
		$\Gamma = 0.7$	$\Gamma = 0.43$
1	150 [kg]*) 13*)	70 [kg]	100 [kg]
2	4.48	4.48	4.48
3	0.8	0.80	0.80
4	0.4	0.8	0.8
5	0.06	0.04	0.06
6	0.002	0.05	0.05
7	0.8	0.6	0.7
8	0.01	0.03	0.03
9	0.01	0.04	0.06
10	0.104	0.104	0.104
11	0.2	0.2	0.07
12	0.3	0.15	0.07
13	0.04	0.004	0.003
14	0.2	0.001	0.001
15	0.03	0.003	0.002
16	0.04	0.002	0.002
17	0.004	0.0002	0.0002

\* ) The diameter before the first separation yields 150 kg, the diameter at the end of the photographed trail (before the separation of No. 7) yields 13 kg.

The dependence in Fig. 15 can be expressed by

$$d = 630 m_E^{0.15}$$

where  $d$  is in cm and  $m_E$  in gr. This relation holds between the diameter of the luminous trajectory and the mass of the meteorite at heights around 30 km and for the meteorite masses in the range from  $10^2$  to  $10^4$  gr.

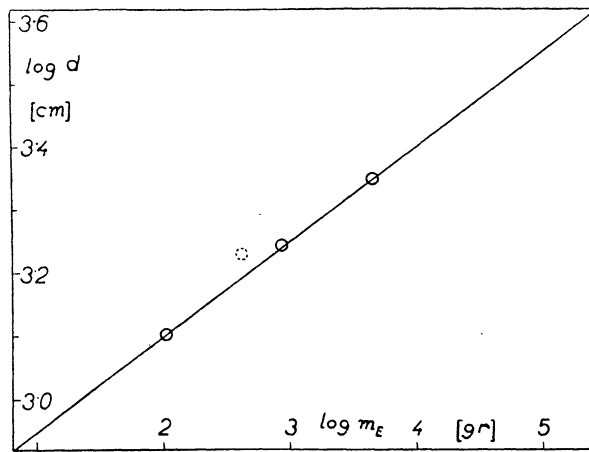


Fig. 15. Diameter  $d$  of the luminous trajectory of the fireball as the function of the meteorite mass  $m_E$  was used for the determination of masses of the not found meteorites from their trajectories.

#### 4.2 "Dynamical" masses

The relations (19) and (20) can be used for the determination of masses of individual meteorites at the points of separation from the parent body. These equations can in this case be written

$$(28) \quad v_B^2 - v_E^2 = C_B(\varrho_B - \varrho_E)$$

$$(29) \quad C_B = -\frac{2\Gamma A v_B^2 m_B^{-1/3}}{b \cos z_R}$$

The difference  $v_B^2 - v_E^2$  and  $\varrho_B - \varrho_E$  are the values, which can be derived from our photographic records. Thus the values  $C_B$  can be computed from (28) and  $m_B$  from (29).

It is possible to compute the total loss of the mass for such trails for which the end mass is given from the mass of found meteorite. The coefficient  $A$  can be determined, assuming that it is constant, from the relation

$$(30) \quad \log m_E = \log m_B - \frac{0.434 \frac{A}{\Gamma} (v_B^2 - v_E^2)}{4Q}$$

The coefficient  $\Gamma$  is used from Table 19. Formally the dependence of the computed  $A$  on the velocity  $v_B$  was supposed. This is of course in contradiction to the supposition of constant  $A$ , that is with equation (30), and can be used as a first approximation only. The ratio  $A/\Gamma$  was thus determined for each trajectory and then the  $m_B$  can be transferred to the values  $m_E$  using relation (30). The numerical results are in Table 21. A great dis-

agreement with the results of Section 4.1 is evident. This disagreement could be explained by the following facts:

- a)  $A$  is not constant
- b)  $v_E$  is a function of the meteorite mass
- c)  $C_B$  is not constant
- d) the diameter of the luminous trajectory depends not only on  $m_E$  but also on  $\varrho$  and  $v$ .

Therefore we must consider all the mass determinations of this paper as roughly preliminary estimates which could be improved in a further paper using some theoretical results about the effects a) to d). For this purpose one of the further papers of this series will be devoted to the problem of the masses of the not found meteorites.

The total mass which fell on the surface in the Příbram multiple meteoritic fall will remain a theoretical value only, until the biggest meteorite is found. The wrong identification in paper [7] led to the belief that a substantial part of the mass was found, and thus the total mass of all meteorites was almost an experimental value. But the correct identification of this paper changes the situation completely, and it is not possible to give an experimentally determined total mass of all the meteorites. Thus it is not possible to make a number of considerations which were published in paper [7].

#### Acknowledgement

My thanks are due to all the members of the Department of the Interplanetary Matter of the Astronomical Institute of Czechoslovakia and to members of other scientific departments of this Institute, who took part in the expedition to the region of the meteorite fall, for their good work in such unusual conditions. I am indebted to all the inhabitants in the region of the meteorite fall who helped in the search for meteorites and who gave us visual data about the fireball. My special thanks are addressed to the finders of meteorites for the care which they dedicated to our work.

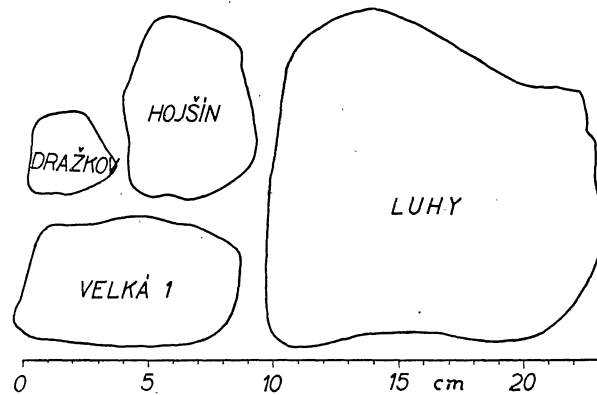


Fig. 16. Head cross-sections of the found meteorites.

I am very much indebted: to M. Ježková and N. Lukašová for their quick preliminary computations and for their careful definitive numerical computations; to J. Šuráň for his valuable advice and practical help with the geodetical measurements; to M. Novák and M. Brož, who obtained the photographs of the meteorite fall by their

precise performance of the service; to L. Straka for the photographic processing of the plates; to driver M. Tlamicha for his devoted transport of members of the expeditions to hardly accessible places. My greatest thanks are due to J. Rajchl and L. Sehnal for their effective help in the organisation of expeditions, the obtaining of visual observations and mainly for the valuable scientific discussions. I am very much indebted to J. G. Davies of the Jodrell Bank Experimental Station for his careful supervision of the paper.

My special thanks are due to V. Guth, who at the time of the meteorite fall was seriously ill, but nevertheless devoted great care to our work.

### *List of mathematical symbols*

$a'$	the semimajor axis of the earth ellipsoid	$D'_\varphi$	the deviation of the vertical projection of the real trajectory from the reference one
$e'$	the eccentricity of the earth ellipsoid	$D_h$	the deviation of the height measured on the real trajectory from the height of the reference trajectory
$\varphi$	the geographic latitude	$\Delta h$	the residuals of the direct double-station heights from the smooth heights
$\lambda$	the geographic longitude	$D$	the perpendicular deviation of a point from the reference trajectory in the vertical projection to the ground
$\varphi'$	the geocentric latitude	$D_M$	the perpendicular deviation of the place of meteorite fall from the vertical projection of corresponding trajectory of the fragment. The sign +: the deviation is directed to the right (north), the sign -: the deviation is directed to the left (south). This holds for $D$ also
$R$	the geocentric radius vector of the zero height above sea-level	$I$	the luminosity of the fireball
$R_r$	the geocentric radius vector of the point on the reference trajectory (the suffix means the point to which the radius vector refers)	$M_v$	the absolute (100 km) magnitude of the meteorite light
$t_s$	the hour angle	$E$	the total radiated energy
$\delta_s$	the declination	$v$	the velocity of the meteorite
$d_{0n,P}$	the distance Ondřejov—Prčice	$v_\infty$	the original velocity of the meteorite
$x_P, y_P, z_P$	the rectangular geocentric coordinates of the Prčice station	$c_v, c_\alpha, c_\delta$	the coefficients defined by equations (17) and (18)
$\vartheta_P$	the local sidereal time of Prčice	$L_H, B_H$	the ecliptical system of coordinates
$\varrho$	the right ascension of the point of intersection of the apparent trajectory (great circle) with the equator	$a, e, q, \omega, \Omega, i, \pi$	the orbital elements
$\psi$	the inclination of the apparent great circle of the trajectory to the equator	$\varrho$	the air density
$\alpha_r$	the right ascension of the reference great circle (6 <sub>2</sub> ) as seen from the Prčice station	$\varrho_0$	the air density at zero height
$l$	the distance of an arbitrary point (break) on the real trajectory of the meteorite from the basic point of the trajectory	$b$	the air density gradient
$l'$	the distance of an arbitrary point (break) measured on the photographed meteorite trail from the basic point	$m$	the mass of the meteorite at height $h$
$k$	the constant of the Millman relation proportional to the distance of the basic point from the station	$m_E = m_s$	the mass of the meteorite at the end of the luminous trajectory and on the surface of the earth
$n$	the distance of the image of the basic point on the plate from the image of the radiant	$\rho_M$	the density of the meteorite material
$h$	the height above sea-level	$A$	the shape coefficient $A = s_E/m_E^{2/3}$
$\Delta l$	the length measured along the trajectory, which corresponds to one break	$s_E$	the head cross-section of the meteorite
$\Delta t$	the duration of one break	$S$	is defined by (25)
$r_0$	the closest distance of the reference trajectory from Prčice	$\Lambda$	the heat transfer coefficient
$\omega_{R,r}$	the angular distance of the radiant from an arbitrary point on the reference trajectory	$\Gamma$	the drag coefficient
$D_\alpha, D_\delta, D_\varphi, D_\lambda, D_\vartheta$	the deviations of the real trajectory from the reference one in the direction of the corresponding coordinate	$C$	the definitions (19) and (20)
		$C_B$	the definition (29)
		$B$	the definitions (21) and (22)
		$g$	the gravitational acceleration
		$v_e$	the component of the meteorite velocity in horizontal direction in the vertical plane of the meteorite trajectory
		$v_h$	the vertical component of the meteorite velocity
		$V$	the wind velocity component against the azimuth of the meteorite flight
		$V_x$	the wind velocity component perpendicular to the trajectory of the meteorite in the horizontal plane
		$L$	the dark-flight distance measured in the projection to the ground from the end point of the luminous trajectory to the place of the meteorite fall
		$M$	the Mach number
		$\Gamma(M)$	$\Gamma$ as the function of the Mach number
		$z$	the zenith distance
		$v_s$	the velocity of the meteorite at its incidence with the surface